

Ph. D. Thesis

***Study on Silicon-Germanium Thermoelectric
Materials Formed by Pulse-Current Sintering of
Gas-Atomized Powders***

Masatoshi Otake

Shizuoka University, Japan

December 2003

Abstract

Silicon-germanium (Si-Ge) alloy has been known as a high-temperature thermoelectric element material, which can perform thermal-electrical energy conversion using the temperature difference between both ends of the element. This alloy has been successfully applied to the power source for artificial satellites and is further expected to be applied for a terrestrial use such in environment-friendly power generation systems utilizing waste heat from energy-related facilities. In this research, gas-atomizing and pulse-current sintering techniques were used to obtain Si-Ge sintered bodies, and the physical and thermoelectric properties of their starting powders and sintered bodies were elucidated. Furthermore, the Si-Ge thermoelectric element and its module were fabricated, followed by the evaluation of their outputs.

First, both semiconducting types of $\text{Si}_{0.8}\text{Ge}_{0.2}$ powders were prepared with boron or phosphorous added into a mixture of Si and Ge by a gas-atomizing method, and then the dense bodies were formed from these two types of Si-Ge powders by pulse-current sintering. The Si-Ge powders were characterized and their sinterability was then studied. Especially, an effect of ball-milling on the sinterability of the powders was discussed. The mean particle sizes of as-prepared p- and n-type Si-Ge powders were 72 and 66 μm , respectively. The mean particle sizes of both types of as-prepared powders were pulverized down to 3.0 and 2.6 μm by ball-milling for 10 h, respectively. Both the decrease in the crystallite size and the increase in the heterogeneous distortion in the particles correlated with the ball-milling time. The densification of as-prepared powders was abruptly promoted above 1500 K, while that densification temperature of the ball-milled powders decreased by approximately 100 K. That is, the sinterability of as-prepared powders was improved with the decrease in the crystallite size and the increased surface distortion mechanochemically introduced by ball-milling. The pulse-current sintering of the gas-atomized powder and its

ball-milled one could yield the shaped bodies with a density of more than 99 % at 1523 and 1433 K, respectively, only in 3min as a soaking time. The grain size and elemental inhomogeneity of the dense bodies were also reduced by the ball-milling.

Secondly, the thermoelectric properties such as the thermal conductivity, κ electrical resistivity, ρ and Seebeck coefficient, S of the dense bodies were determined at from room temperature to 1073 K. The effect of ball-milling on the thermoelectricity was also discussed. The thermoelectricity was evaluated by $ZT (=S^2T/\rho\kappa)$, which is so called “figure of merit”. An effective thermoelectric material should possess larger Seebeck coefficient, lower electrical resistivity and lower thermal conductivity. The ball-milling was expected to decrease the thermal conductivity then to improve the thermoelectricity. As expected, the thermal conductivities of p- and n-type Si-Ge dense bodies were decreased by 8 and 10% on average between 300 and 1073 K, respectively by ball-milling. However, this phenomenon was accompanied with an increase in electrical resistivity due to the reduced grain size and increased oxygen content, resulting in the decrease in thermoelectricity by 13 and 8% for p- and n-type Si-Ge dense bodies, respectively. The thermoelectricity of n-type Si-Ge exceeded that of p-type Si-Ge because of the high Seebeck coefficient of n-type samples. Finally, the largest ZT value of 0.66 was obtained for the Si-Ge dense body from the n-type gas-atomized powder. It was found that the application of the gas-atomized powder for fabricating Si-Ge sintered body has the advantage of the reduction in oxygen content and in resistivity compared to the case of the pulverized powders.

Thirdly, two types of p-n joined $\text{Si}_{0.8}\text{Ge}_{0.2}$ thermoelectric elements were fabricated by pulse-current sintering of the corresponding gas-atomized powders: One joined element was obtained by making a slit between the p- and n-type dense bodies after the sintering, and the other element had an alumina layer sandwiched instead of a slit for strengthening. The p-n junctions of both elements were firmly connected without any crack. The alumina layer inserted existed likewise as it had been even after sintered, which may be attributed to a very short pulse-current sintering time. The influence of the configuration; length of

element l , depth of slit l_i , and width of element leg w on the maximum output was studied. Five joined elements with a slit and one with an alumina layer were fabricated according to the various preset configurations to evaluate comparatively the output at a temperature of 1273 K. The outputs of these elements were largely dependent on their configurations. The configuration of $l=26$ mm, $l_i=23.5$ mm, and $w=2.5$ mm gave the maximum outputs of 46 and 49 mW without and with an alumina layer, respectively. It was shown that the insertion of an alumina layer increased the output the thermoelectric element. The penetration behavior of dopants, boron and phosphorous across a p-n junction in a joined Si-Ge semiconductor was also elucidated by x-ray photoelectron spectroscopic analysis. An interlayer with a thickness of approximately 2 mm was found in the p-type side. For obtaining higher output, 20-layered Si-Ge element and Si-Ge thermoelectric module which consists of 16 of ceramic-inserted joined Si-Ge elements were then fabricated, which showed the maximum outputs of 122 mW and 2.0 W, respectively.

It was concluded that the combination of gas-atomizing and pulse-current sintering techniques was effective to fabricate Si-Ge dense body and p-n joined element in speedy and simple process compared to the conventional way. It is expected that the obtained techniques would be the aid of the spread of the Si-Ge and other thermoelectric materials for their terrestrial and commercial use.

Contents

Abstract	I
Acknowledgements	VII
Chapter 1 Introduction	1
1.1 Thermoelectric materials	1
1.2 Silicon-germanium semiconductor	3
1.3 Gas-atomizing and pulse-current sintering techniques	7
1.4 Research objectives	9
References.....	10
Chapter 2 Characterization and Sintering of Si-Ge Powders	13
2.1 Introduction	13
2.2 Experimental	
2.2.1 Sample preparation	14
2.2.2 Characterization	15
2.3 Results and discussion	
2.3.1 Characteristics of powder	15
2.3.2 Densification	19
2.3.3 Microstructure and element distribution of sintered bodies.....	21
2.3.4 Morphology of sintered bodies	23
2.4 Summary	24
References	25

Chapter 3	Thermoelectric Properties of Si-Ge Dense Bodies	27
3.1	Introduction	27
3.2	Experimental	
3.2.1	Sample preparation	27
3.2.2	Characterization	28
3.3	Results and discussion	
3.3.1	Thermoelectric properties	29
3.3.2	Figure of merit	34
3.4	Summary	38
	References	38
Chapter 4	p-n Joined Si-Ge Thermoelectric Element	41
4.1	Introduction	41
4.2	Experimental	
4.2.1	Fabrication of joined element	42
4.2.2	Characterization and evaluation.....	44
4.3	Results and discussion	
4.3.1	Joined element	46
4.3.2	Output of joined element	49
4.4	Summary	52
	References	53
Chapter 5	XPS Analysis of p-n Junction	55
5.1	Introduction	55
5.2	Experimental	
5.2.1	Sample preparation	55
5.2.2	XPS analysis	56
5.3	Results and discussion	
5.3.1	Binding energy.....	57

5.3.2 Formation of interlayer	59
5.4 Summary.....	61
References	62
Chapter 6 Multilayered Si-Ge Thermoelectric Element and Module	63
6.1 Introduction.....	63
6.2 Experimental	
6.2.1 Fabrication of multilayered element and module.....	64
6.2.2 Measurement of output	65
6.3 Results and discussion	
6.3.1 Multilayered element	65
6.3.2 Comparison with module.....	68
6.4 Summary	71
References	71
Chapter 7 Conclusions	73
List of Papers and Presentations	75

Acknowledgments

I would like to express my sincere appreciation to my supervisor Professor Shoji Kaneko to his guidance, encouragement and valuable discussion throughout this research. Special thanks are due to Professor Akifumi Ueno, Professor Tatsuo Fujinami, Professor Motoki Nakamura, Assistant Professor Kenji Murakami and Professor Kunihito Komoto (Nagoya University) for their critical reading of the manuscript and valuable comment.

I wish to express my thanks to Mr. Takayoshi Shimizu and Dr. Koich Morii of Daido Steel Company for their assistance in the preparation of gas-atomized powders. I also wish to thank Mr. Hisashi Ito, Mr. Mamoru Anma and Dr. Akio Kawabe of Shizuoka Industrial Research Institute and Dr. Osamu Sugiyama of Fuji Industrial Research Institute as well as Mr. Kenji Sato and other researchers of Hamamatsu Industrial Research Institute for appreciation of my research.

I am very delighted to acknowledge my wife Yoshiko and my daughter Mai for their love and encouragement throughout my endeavor over the past years.

Chapter 1 Introduction

1.1 Thermoelectric materials

Thermoelectric phenomena included Seebeck, Peltier and Thomson effects were all discovered in the early-nineteenth century.¹⁾⁻³⁾ In 1823 Seebeck reported the effect that an electric current flow around a closed circuit made up of different electrical conductors when the junctions are subject to different temperatures. For small temperature differences, the generating voltage is found to be proportional to the temperature difference. Some 12 years later, a complementary effect was discovered by Peltier, who observed temperature changes in the vicinity of the junction between dissimilar conductors when current passed. This absorbing or releasing heat in the junction was found to be proportional to the magnitude and duration of the external current applied. In 1851 Thomson predicted the existence of third thermoelectric effect; absorption or release of heat occurred when an electric current passes through a single homogeneous conductor in the presence of a temperature gradient. This heat is proportional to the magnitude and duration of the current and to the temperature difference. However, substance that showed large thermoelectric phenomena was not discovered because metals were considered to be an only conductor in this age.

Renewed interest in thermoelectricity occurred in the late 1930s accompanied with the development of semiconductor's synthesis, then in the late 1950s and early 1960s, considerable research was devoted to a search of effective thermoelectric materials.²⁾ For the purpose of evaluation of thermoelectricity, it is convenient to define the figure of merit Z for a single material as^{3),4)}

$$Z = S^2 / \rho\kappa, \quad (1.1)$$

where ρ and κ are the electrical resistivity and thermal conductivity, respectively. The equation (1.1) indicates that good thermoelectric materials should possess large Seebeck coefficient, low electrical resistivity and low thermal conductivity. Since Z vary with the temperature T , it is more useful to multiply Z by T as

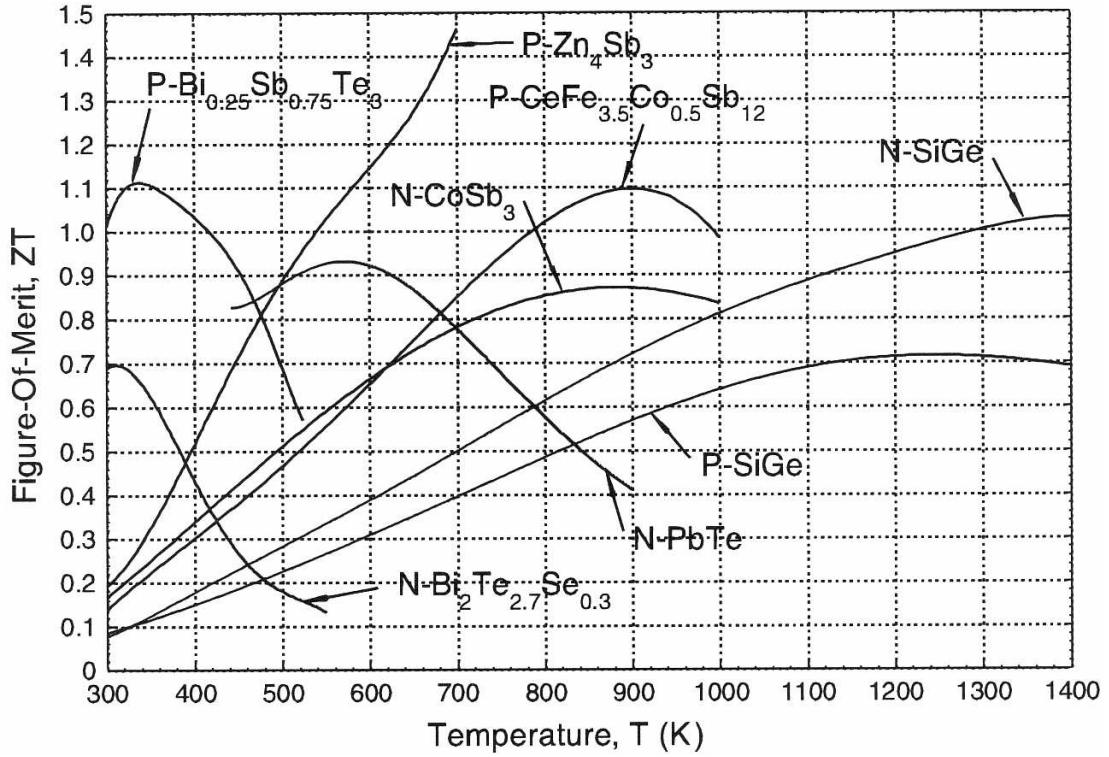


Fig. 1.1. Figure of merit ZT of some thermoelectric materials.¹¹⁾

$$ZT = S^2 T / \rho \kappa, \quad (1.2)$$

where ZT is dimensionless figure of merit and T is the absolute temperature. The maximum efficiency ζ of conversion of heat to electrical energy under optimum current load condition is given by^{3),4)}

$$\zeta = ((T_h - T_c) / T_h) (((1 + ZT_{mean})^{1/2} - 1) / ((1 + ZT_{mean})^{1/2} + T_c / T_h)) \quad (1.3)$$

where T_h and T_c are the temperatures of hot and cold part of the thermoelectric material, respectively, and T_{mean} is $(T_h + T_c)/2$. Thus, the conversion efficiency increases as increasing ZT .

Well-known thermoelectric materials are bismuth telluride (Bi_2Te_3)⁵⁾ for the low temperatures ($\sim 300^\circ\text{C}$), lead telluride (PbTe)⁶⁾ and cobalt triantimonide (CoSb_3)⁷⁾ for the medium temperatures ($\sim 600^\circ\text{C}$) and silicon-germanium (Si-Ge)⁸⁾ iron disilicide (FeSi_2)⁹⁾ and some thermoelectric oxides such as NaCo_2O_4 ¹⁰⁾ for the high temperatures ($\sim 1000^\circ\text{C}$). The figure of merit ZT changes depending on the temperature, and each material has its own range of useful operating temperatures, as shown in **Fig. 1.1**.¹¹⁾ These thermoelectric

materials have a function of thermal-electrical energy conversion using of the temperature difference between both ends of the bodies, and can be applied for a thermoelectric power generator or a thermoelectric cooling/heating apparatus by making use of Seebeck and Peltier effect, respectively. Practically, thermoelectric materials are generally used as “thermoelectric module” composed of lots of thermoelectric elements which is fabricated by connecting one side of p- and n-type semiconductors with metal plate, as shown in **Fig. 1.2.**⁴⁾ Because thermoelectric effects are electronic in nature, these thermoelectric apparatus have many advantages such as 1) no moving parts 2) silent operation 3) potential long life 4) maintenance free.²⁾ Bi_2Te_3 has been widely used as cooling of electronic devices, domestic food refrigerators or numerous other cooling applications,¹²⁾ while PbTe and Si-Ge has been used as long-life, maintenance-free and remote power sources for isolated locations such as in a desert, sea,¹³⁾ or space.¹⁴⁾

1.2 Silicon-germanium semiconductor

Both silicon and germanium are the best known and most well understood

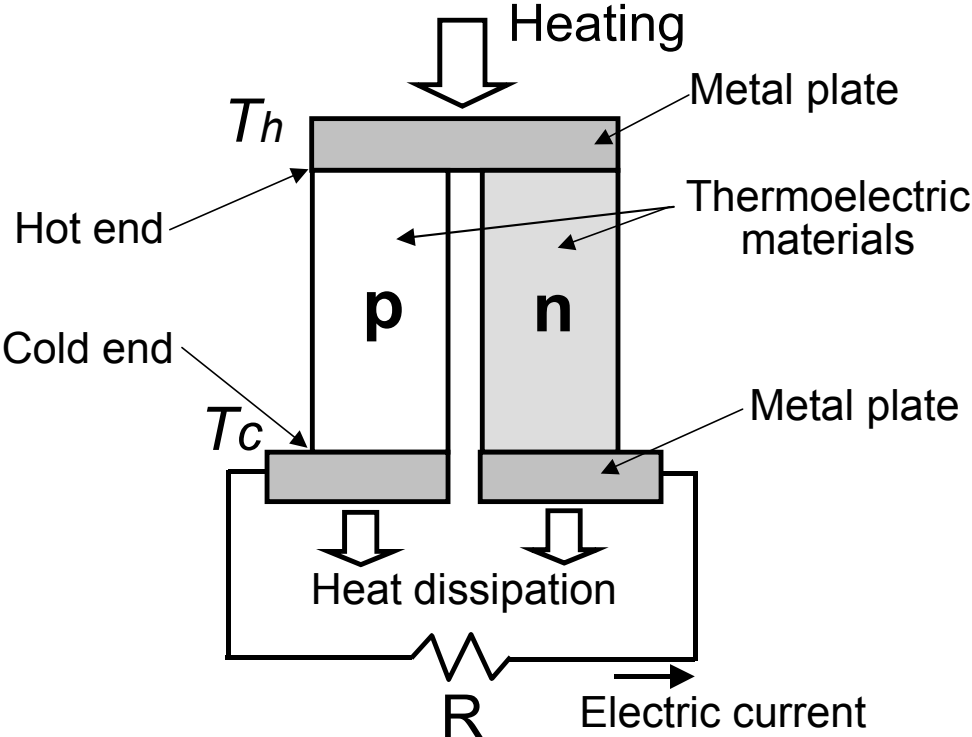


Fig. 1.2. Illustration of thermoelectric element.

materials which have been investigated for a number of semiconductor device applications. The physical properties of silicon and germanium are shown in **Table 1.1**.^{2),15)} The high melting points, large energy gaps and resistance to atmospheric oxidation would suggest that they are suitable candidates for high-temperature thermoelectric materials. However, thermal conductivities are too high and consequently the figures of merit are low. In the early 1960s, the discovery that Si-Ge alloys have a low thermal conductivity at high temperatures¹⁶⁾ has led to an investigation of these alloys for thermoelectric power generations.^{17),18)} The lattice thermal conductivity of Si-Ge alloys (Si-20 mol%Ge) decrease by approximately 90 %, as shown in **Fig. 1.3**.⁴⁾ **Figure 1.4** indicates the composition dependence of the dimensionless figure of merit ZT for Si-rich alloys,⁸⁾ from which $\text{Si}_{0.8}\text{Ge}_{0.2}$ was determined as the optimized composition. Silicon and germanium are completely miscible in both the liquid and solid states, however, a large separation exists between the liquidus and the solidus, as shown in **Fig. 1.5**.¹⁹⁾ Cast ingots typically exhibit severe alloy segregation, thus, powder metallurgical methods are generally preferred for production of significant quantities of Si-Ge.⁸⁾ For this reason, the Si-Ge thermoelectric elements were mostly made by hot pressing of powders obtained by pulverizing the corresponding ingots, as shown in **Fig. 1.6**.

Table 1.1. Physical Properties of Si, Ge and $\text{Si}_{0.8}\text{Ge}_{0.2}$ ²⁾

			Si	Ge	$\text{Si}_{0.8}\text{Ge}_{0.2}$
Structure			Diamond		
Melting point	K		1693	1209	1550
Energy gap	eV		1.1	0.7	1.0
Mobility	Electron	$\text{cm}^2\text{V}^{-1}\text{S}^{-1}$	1300	4500	400
	Hole	$\text{cm}^2\text{V}^{-1}\text{S}^{-1}$	500	3500	250
Lattice thermal conductivity	$\text{Wm}^{-1}\text{K}^{-1}$		150	60	4
Density	10^3kgm^{-3}		2.33	5.32	2.99
Thermal expansion	at 300K		4.2	6.1	4.2
Compressive strength	p-type at 300K	MPa	-	-	653
	n-type at 300K	MPa	-	-	473
Tensile strength	p-type at 300K	MPa	-	-	201
	n-type at 300K	MPa	-	-	129

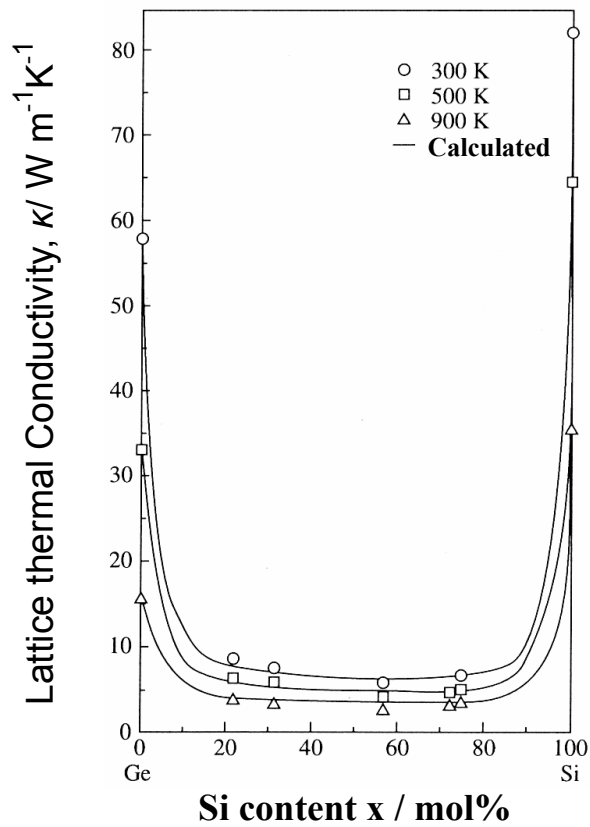


Fig. 1.3. Lattice thermal conductivity of $\text{Si}_x\text{Ge}_{1-x}$ alloys.⁴⁾

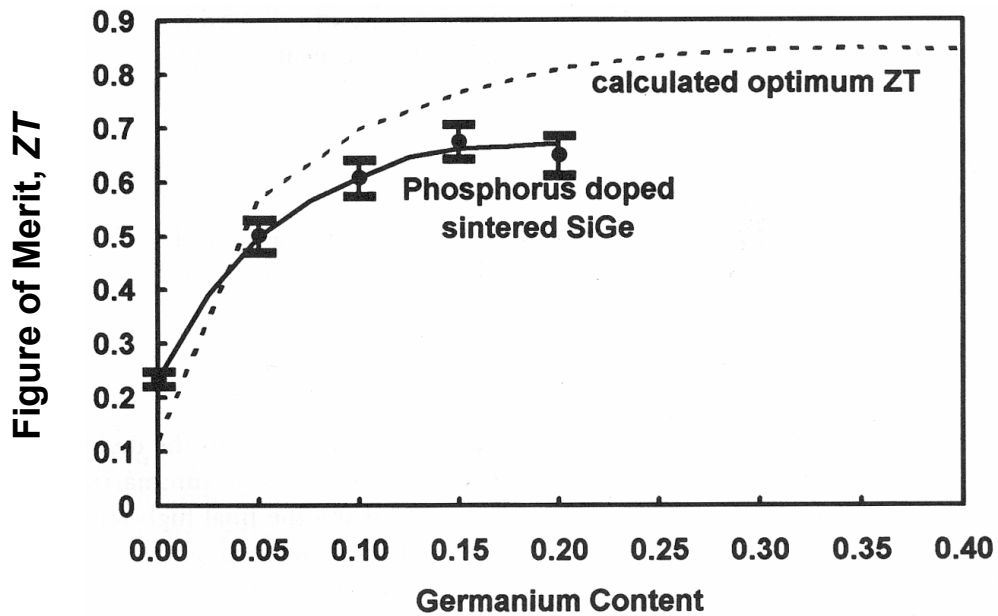


Fig. 1.4. Germanium content dependence of $\text{Si}_{1-x}\text{Ge}_x$ alloys on the figure of merit ZT .⁸⁾

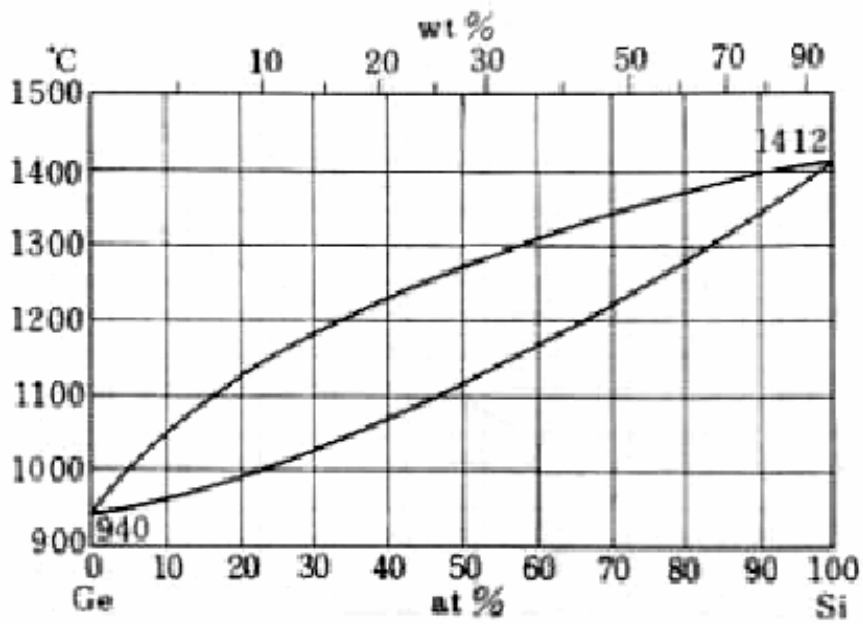


Fig. 1.5. Phase diagram of Si-Ge system.¹⁹⁾

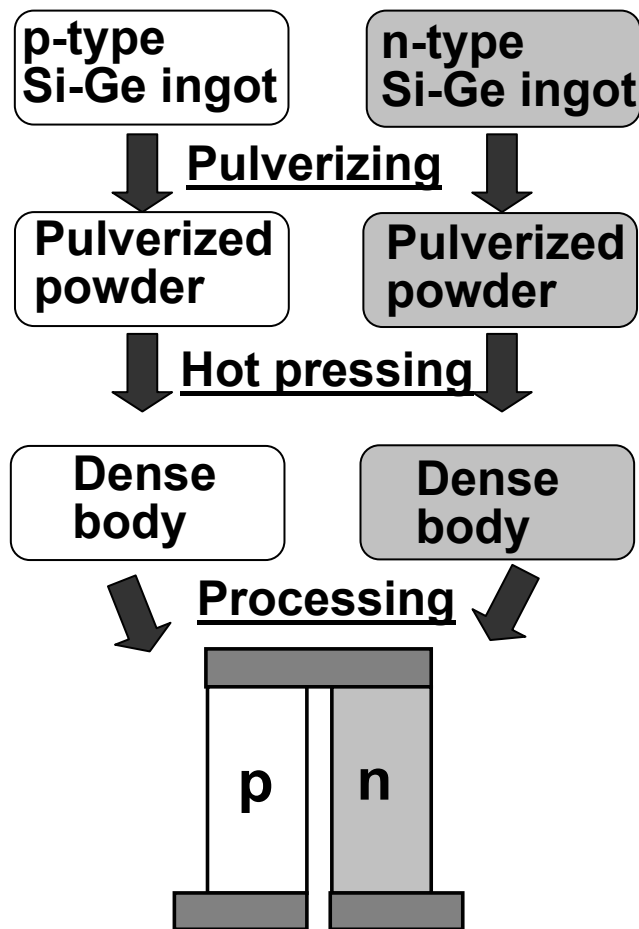


Fig. 1.6. Processing of Si-Ge thermoelectric element.

A radioisotope thermoelectric generator (RTG) which used radioisotopes as a heat source was successfully applied to the power source for the artificial satellite by making use of Si-Ge thermoelectric element.¹⁴⁾ The most commonly used radioisotope, ²³⁸Pu has a half-life of 87.8 year and decays by the emissions of alpha particles as producing the heat. The experimental satellites (LES8 and LES9) launched in 1976, the Voyager 1 and 2 spacecrafts in 1977, the Galileo spacecrafts in 1989 and Ulysses spacecrafts in 1990 were all equipped by this RTG.¹⁴⁾ Especially, the RTG's of the Voyager 1 and 2 spacecrafts have been operating for more than twenty five years.

1.3 Gas-atomizing and pulse-current sintering techniques

A gas-atomizing technique is suitable for production of homogeneous metal or metallic alloy powders.²⁰⁾ As, shown in **Fig. 1.7**, the melt stock in the form of elemental or

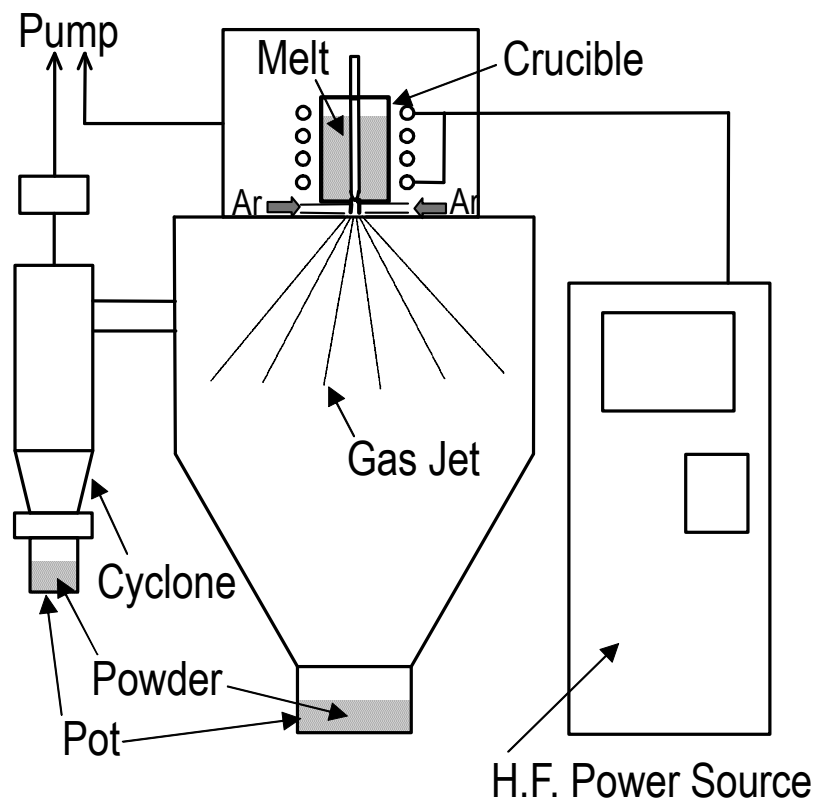


Fig. 1.7. Apparatus of gas-atomizing process.

multi-element metallic alloys in the crucible is melted by an induction, arc, or other type of furnaces. After the bath is melted and homogenous, the melt is dropped into the atomizing chamber through the nozzle under the crucible. As the metal stream exits the nozzle, it is struck by a high velocity stream of an inert gas. The molten metal stream is broken down into fine droplets which solidify during their fall through the atomizing tank. Particles are collected at the bottom of the tank. Gas-atomized powders are typically spherical and have smooth surfaces.²¹⁾ The particle size decreases with increasing gas pressure.²²⁾ The atomizing technique has been used for a wide range of alloys, such as stainless steels, low alloy steels, copper alloys as well as the low melting temperature materials such as aluminum, lead, tin, zinc and their alloys.²³⁾

Pulse-Current Sintering (PCS), which was commercially called Spark Plasma Sintering (SPS) or Plasma Activated Sintering (PAS), is a new and unique densification technique developed in 1988-1990.²⁴⁾ PCS is a kind of hot pressing which employs a low voltage and

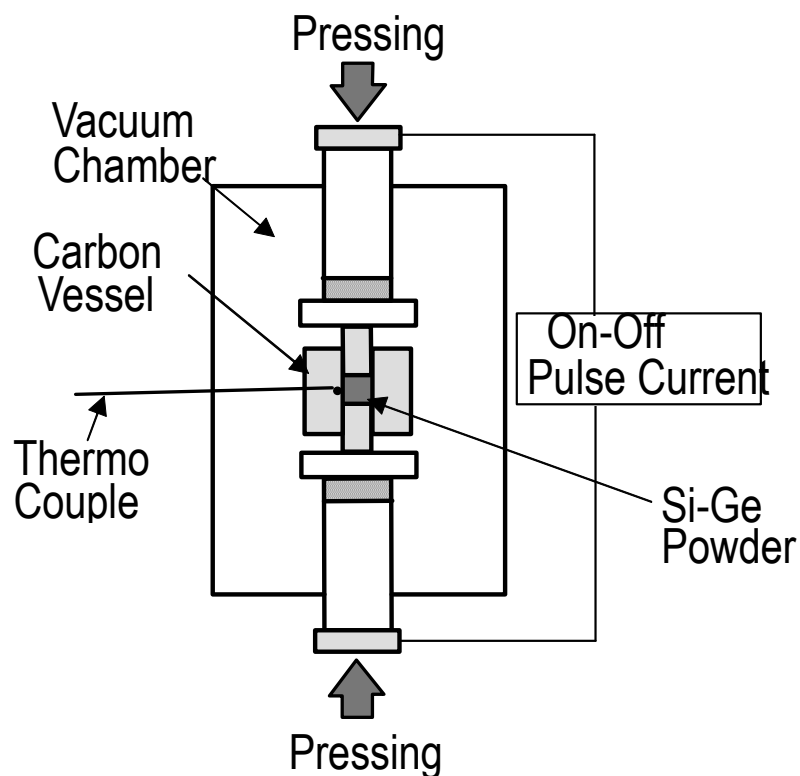


Fig. 1.8. Apparatus of pulse-current sintering system.

high electric current in a pulse shape as the heat source under uniaxial pressure.²⁵⁾ This process can yield a dense body of a wide range of metals, ceramics and polymers in a very short period compared to other hot pressing processes.²⁶⁾ It is also suitable for sintering or joining process which need to suppress grain growth, diffusion and crystallization.²⁴⁾ **Figure 1.8** shows the main components of the PCS apparatus (SPS-1030, Sumitomo Coal Mining Co. Ltd., Japan). A powder is placed in the die which is made of electrically conductive materials without any binder and compressed by punches. Then, DC pulse-current is supplied to the die and powder for sintering under pressing. Pulse-current may play an important role as a trigger for sintering at many contact points between particles.²⁷⁾ It was reported that the oxide layers of aluminum powders were fractured by this process.²⁸⁾

1.4 Research objectives

As previously described, thermoelectric power generation has been successful in application in space. On the other hand, thermoelectric materials have not been used for terrestrial power generation except for some special use. Especially in Japan, only Bi_2Te_3 was commercially used for thermoelectric cooling. The studies for thermoelectric power generation were not conducted sufficiently due to both a good supply of electricity and an absence of space industry in this country. However, in recent years, the researches using a waste heat as a new energy source are also in progress due to a serious problem of energy and the increasing interest in the environment. Attempts to collect a waste heat by means of thermoelectric generator using Bi_2Te_3 for low temperatures and PbTe for medium temperatures were reported. However, the disadvantages of these materials are that deposits of these raw materials are small, and some of them are toxic, and they are not available in applications in high temperatures in air. Si-Ge alloys are non-toxic and can be used in the wide temperature range till about 1300 K, although they are rather expensive because of germanium.

Si-Ge has not been used as a commercial use yet due to the low cost-performance

originated from the high manufacturing cost, which may be attributed to not only the expensive germanium but also long and complicated process including the production of powder, sintering process and fabrication of the element and module. The gas-atomizing process is superior to the pulverizing process for producing large-lots of uniform powder without contamination in a short period. The PCS process can yield dense bodies in 1-3 min as soaking time, while conventional hot-pressing process need longer sintering time such as 1h. Thus, it may be effective for both process simplification and cost reduction to use these gas-atomizing and PCS techniques. In addition, the PCS technique may enable us to produce p-n joined Si-Ge semiconductor in one process by simultaneous joining and sintering of p- and n-type powders, which makes the conventional joining process needless.

First, p- and n-type Si-Ge powders and their sintered bodies were obtained by using gas-atomizing and pulse-current sintering technique. The characteristics and sinterability of the powders including characteristics of the dense bodies were investigated. Secondly, the thermoelectricity of obtained p- and n-type Si-Ge dense bodies was elucidated by determining the Seebeck coefficient, electrical resistivity and thermal conductivity. Finally, p-n joined Si-Ge thermoelectric element was fabricated in one process by pulse-current sintering and then the outputs of the elements and thermoelectric module were evaluated.

References

- 1) Rowe, D. M., "CRC Handbook of Thermoelectrics," Ed. by Rowe, D. M., CRC Press, London, U. K. (1995) pp.1-5.
- 2) Wood, C., *Rep. Prog. Phys.*, Vol.51, pp.459-539 (1988).
- 3) Goldsmid, H. J., "CRC Handbook of Thermoelectrics," Ed. by Rowe, D. M., CRC Press, London, U. K. (1995) pp.19-25.
- 4) Nishida, I., "Thermoelectrics, Principals and Applications," Ed. by Sakata, R., Realize, Tokyo (2001) pp.186-195. [in Japanese]
- 5) Scherrer, H. and Scherrer, S., "CRC Handbook of Thermoelectrics," Ed. by Rowe, D.

- M., CRC Press, London, U. K. (1995) pp.211-237.
- 6) Fano, V., "CRC Handbook of Thermoelectrics," Ed. by Rowe, D. M., London, CRC Press (1995) pp.257-266.
 - 7) Uchida, H., Crnko, V., Tanaka, H, Kasama, A., Itsumi, Y. and Matubara, K., *J. Jpn. Int. Metal*, Vol.**63**, pp.1454-1460 (1999). [in Japanese]
 - 8) Vining, C. B., "CRC Handbook of Thermoelectrics," Ed. by Rowe, D. M., CRC Press, London, U. K. (1995) pp.329-337.
 - 9) Groß, E., Riffel, M. and Stöhrer U., *J. Mater. Res.*, Vol.10, pp.34-40 (1995).
 - 10) Ohtaki, M., *Netsusyori*, Vol.**41**, pp.114-122 (2001). [in Japanese]
 - 11) El-Genk, M. S., Saber, H. H. and Caillat, T., *Energy Conversion and Management*, Vol.**44**, pp.1755-1772 (2003).
 - 12) Goldsmid, H. J., "CRC Handbook of Thermoelectrics," Ed. by Rowe, D. M., CRC Press, London, U. K. (1995) pp.617-619.
 - 13) Hall, W. C., "CRC Handbook of Thermoelectrics," Ed. by Rowe, D. M., CRC Press, London, U. K. (1995) pp.503-513.
 - 14) Rowe, D. M., *J. Power Sources*, Vol.**19**, pp.247-259 (1987).
 - 15) "Netsuden-Handotai," Ed. by Suga. Y., Maki Shoten (1966). [in Japanese]
 - 16) Abeles, B., *Physical Review*, Vol.**131**, pp.1906-1911 (1963).
 - 17) Dismukes, J. P., Ekstrom, L., Steigmeier, F., Kudman, I. and Beers, D.S., *J. Appl. Phys.*, Vol.**35**, pp.2899-2907 (1964).
 - 18) Abeles, B. and Cohen, R. W., *J. Appl. Phys.*, Vol.**35**, pp.247-248 (1964).
 - 19) "Kinzoku Data Book 3rd ed.," Ed. by Nihon Kinzoku Gakkai, (1993) pp.545. [in Japanese]
 - 20) Miller, S. A., Feingold, E. and Vining, C. B., *Modern Developments in Powder Metallurgy*, Vol.**17**, pp.671-682 (1985).
 - 21) Lowley, A., *J. Metals*, Vol.**33**, pp.13-18 (1981).
 - 22) Helmersson, G., Hede, A., Johannesson, T., Bergman, B., Hallen, H. and Burgdorf, K.,

“Advances in Powder Metallurgy & Particulate Materials-1996”, Ed. by Terry Cadle and K S Narasimhan, Metal Powder Industries Federation, Princeton New Jersey, USA (1996) pp.1-109-1-124.

- 23) Adler, A., *Iron and Steel Engineer*, Vol.48, pp.69-76 (1971).
- 24) Yanagisawa, T., Hatakeyama, T. and Matuki, K., *Materia. Jpn.*, Vol.33, pp.1489-1496 (1994). [in Japanese]
- 25) Omori, M., *Mater. Sci. Eng.*, Vol.A287, pp.183-188 (2000).
- 26) Kim, H. T., Kawahara, M. and Tokita, M., *Powder and Powder Metallurgy*, Vol.47, pp.887-891 (2000).
- 27) Murayama, N., *Ceramics Jpn.*, Vol.32, pp.445-449 (1997). [in Japanese]
- 28) Nagae, T., Yokota, M., Nose, M., Tomida, S., Kamiya, T. and Saji, S., *Mater. Trans.*, Vol.43, pp.1390-1397 (2002).

Chapter 2 Characterization and Sintering of Si-Ge Powders

2.1 Introduction

Si-Ge thermoelectric elements were mostly made by hot pressing of powders obtained by pulverizing the corresponding ingots.¹⁾⁻⁴⁾ Here, the sinterability of pulverized thermoelectric material is quite significant because many physical properties on the thermoelectricity such as electrical resistivity and thermal conductivity are firmly connected to the density of shaped bodies. Vining et al. fabricated Si-Ge dense bodies of $2.87\text{-}3.05 \times 10^3 \text{ kg m}^{-3}$ in density by hot pressing of powders with various grain sizes ranging from 1-100 μm .⁵⁾ Beatty and coworkers obtained dense bodies of the density of more than 98% by the same sintering process from ultra-fine (5 to 10 nm) Si-Ge powders.^{6),7)}

An atomizing technique suitable for the production of homogeneous metal or metal alloy powders⁸⁾⁻¹⁰⁾ has also been applied to the preparation of Si-Ge powders. A Si-Ge dense body obtained by hot pressing of atomized fine powders gave the reduction of the inhomogeneity on the Si and Ge distribution.¹¹⁾ However, the characterization and sinterability of gas-atomized Si-Ge powders have not been studied in detail.

Pulse-current sintering (PCS) is a recently developed densification technique by delivering on-off DC pulse electric current to powders under pressing.¹²⁾⁻¹⁴⁾ Pulse current may play an important role as a trigger for sintering at many contact points between particles. It can yield a dense body of metals or ceramics in a very short period compared with other hot pressing processes. Noguchi obtained a shaped body of density greater than 99% for 1 min as sintering soak time from poorly sinterable Si-Ge powders by this technique.¹⁵⁾

In this chapter, semiconducting Si-Ge powders were obtained by gas-atomizing of the melt, followed by densification using PCS technique. The effect of ball-milling on the sinterability of gas-atomized Si-Ge powders was then discussed based on the powder characterization.

2.2 Experimental

2.2.1 Sample preparation

A mixed powder of 80 mol% Si and 20 mol% Ge was doped by adding 0.2 mol% B and 0.3 mol% P for p- and n-type semiconductor formations, respectively. After melting with a microwave-heating furnace in vacuo, the powder was atomized from a nozzle with compressed argon. As-prepared Si-Ge powder was further pulverized by a Fritsch planetary ball-mill at 400 rpm in argon.

A powder sample of 3 g was charged into a cylindrical carbon vessel with an inner diameter of 20 mm, and then uniaxially compressed with a carbon punch at 49 MPa. The sintering was carried out to fabricate a compact for a soaking time of 180 s in vacuo, providing a pulse current of approximately 2000 A and 3 V. The sintering temperatures of as-atomized and pulverized powder were 1473 to 1533 K and 1273 to 1513 K, respectively. The carbon vessel was enclosed with a carbon thermal insulator to realize a temperature uniformity of the charged powder. The sintering temperature was measured with a Pt-(Pt-13 %Rh) thermocouple, the top of which was inserted into the vessel wall adjacent to the sample. Sintered bodies from p-type and n-type as-prepared powders were labeled A_p and A_n , respectively, and those from pulverized powders, P_p and P_n , respectively, as shown in Table 2.1.

Table 2.1. Sintered Bodies

Starting Powder	Chemical Composition	Dopant	Type	Sample Name
As-atomized Powder	$Si_{0.8}Ge_{0.2}$	B	p	A_p
		P	n	A_n
Pulverized Powder		B	p	P_p
		P	n	P_n

2.2.2 Characterization

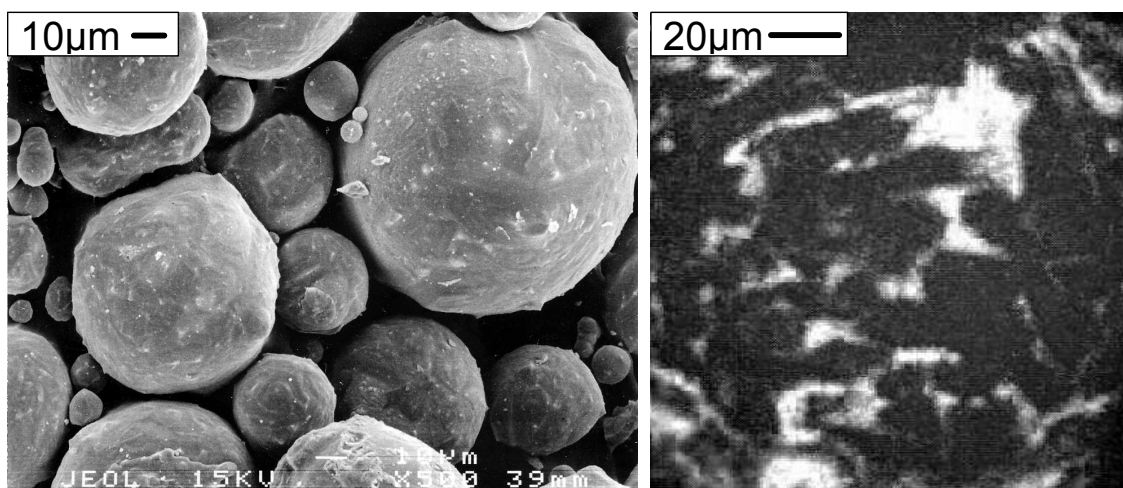
Quantitative analyses of elements of as-prepared powders were carried out by the following methods: Gravimetric method of silicon dioxide for Si, inductively coupled plasma-atomic emission spectrometry (ICP) for Ge and B, and molybdenum blue spectrophotometric method for P. The size distribution of the powder was obtained by a laser diffraction method. The density of the sintered body was measured by an Archimedes method and the microstructure of the body surface was observed after etching with reagent ($\text{HNO}_3+\text{HF}+\text{H}_2\text{O}=5:5:1$). The transverse rupture strength was determined by the span of 10 mm from the sample of $2.5\text{ mm}\times 3.0\text{ mm}\times 15\text{ mm}$ which was cut from the sintered body. The morphology of the powder and fracture surface was observed by SEM. Determination of the crystalline phase and elemental analysis of both powders and sintered bodies were carried out by XRD and EPMA, respectively. Oxygen contents of the powder and sintered body were determined by measuring carbon dioxide generated from the melted sample in a carbon crucible.

2.3 Results and discussion

2.3.1 Characteristics of powder

The chemical compositions of as-prepared powders obtained here were Si 79.7 mol%, Ge 20.1 mol% and B 0.21 mol% for p-type Si-Ge, and Si 79.8 mol%, Ge 20.0 mol% and P 0.18 mol% for n-type Si-Ge. The decrease of phosphorous of the n-type powder by 40% compared with the batch composition was probably due to its volatility with high vapor pressure when melted.

As-prepared n-type powder of relatively large spherical particles was observed in **Fig. 2.1(a)**. The compositional inhomogeneity of Ge was observed on the surface of the powder (**Fig. 2.1(b)**), although a solid solution should be completely formed in the whole composition.¹⁶⁾ It is considered that the segregation of Si- and Ge-rich phases occurred during the cooling stage after Si and Ge starting powders were melted to form a solid



(a) SEM image (b) Mapping image of Ge

Fig. 2.1. SEM image (a) and mapping image of Ge (b) of as-prepared Si-Ge powder. Light gray: Ge-rich phase.

solution. This phenomenon may be attributed to the low rate of diffusion of Ge in the Si-rich phase;¹¹⁾ nevertheless, a gas-atomizing process seems to be one of the quenching methods. As-prepared p- and n-type powders were relatively large particles with mean sizes of 72 and 66 μm , respectively, as shown in **Fig. 2.2**. **Figure 2.3** shows the SEM images of pulverized powders after ball-milling for 1, 10 and 50 h. All pulverized powders were composed of various figures, which were partly flocculated. The size distributions of as-prepared powders were shifted to less than 5 μm of the mean size by pulverizing for 10 h, as shown in **Fig. 2.4**. However, two peaks of approximately 1.5 and 15 μm of the distribution appeared by the ball-milling for 50 h. The appearance of the peak of 15 μm was attributed to the flocculation due to an increase in the surface energy of the powder by prolonged ball-milling time. Consequently, the mean particle size of the powder decreased until 10 h, while it increased thereafter, as shown in **Table 2.2**. Therefore, the densification was hereafter carried out using the p- and n-type powders ball-milled for 10 h, of which the mean particle sizes were 3.0 and 2.6 μm , respectively.

Figure 2.5 shows the XRD patterns of pulverized n-type powders after ball-milled for 1-100 h. It has been proven that all the XRD profiles originate from $\text{Si}_{0.8}\text{Ge}_{0.2}$ because they

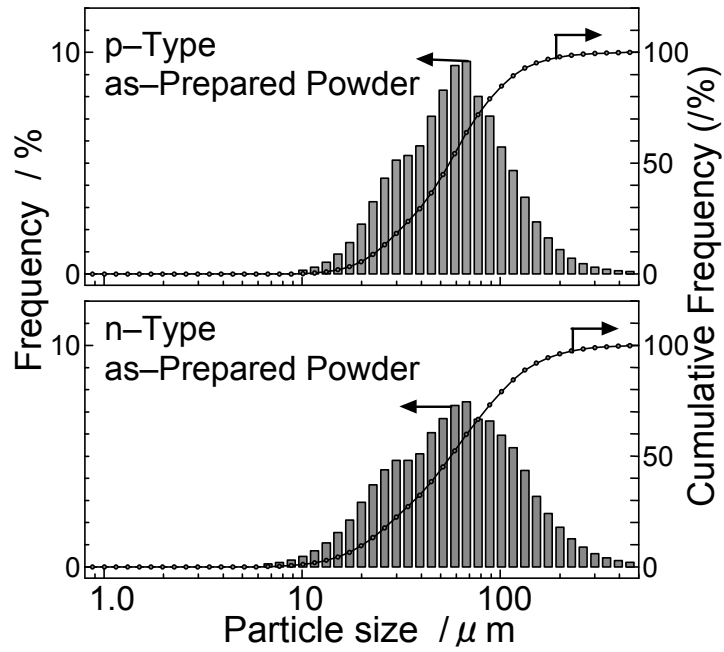


Fig. 2.2. Particle size distributions of p- and n-type as-prepared powders.

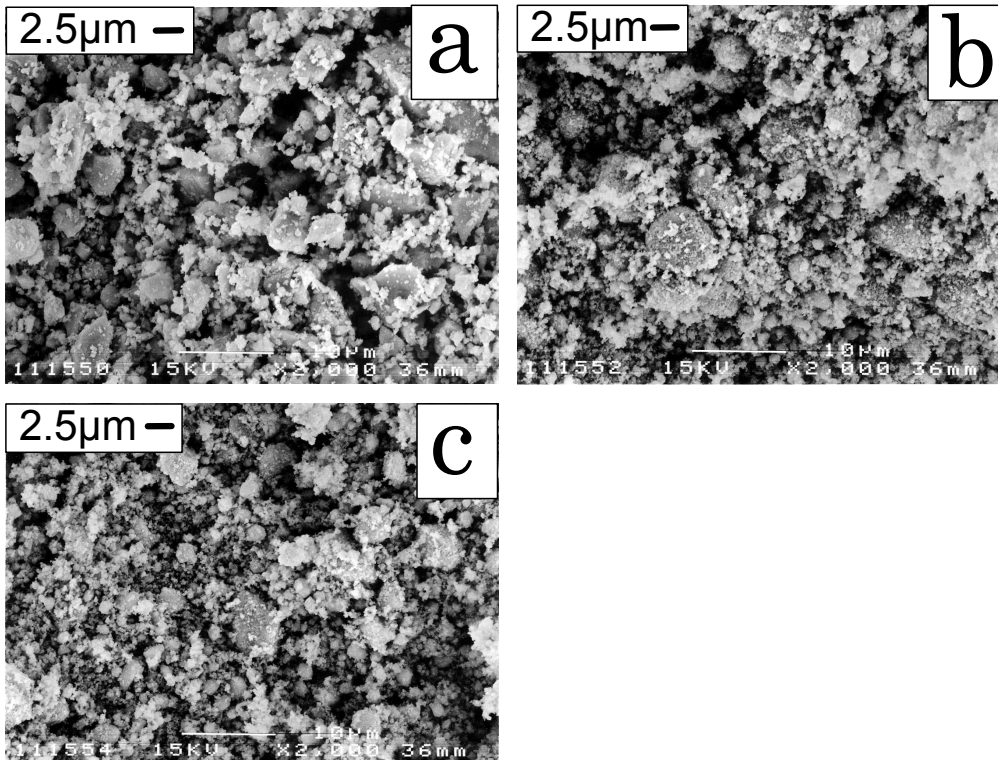


Fig. 2.3. SEM images of n-type pulverized Si-Ge powders ball-milled for (a)1 h, (b)10 h, and (c)50 h.

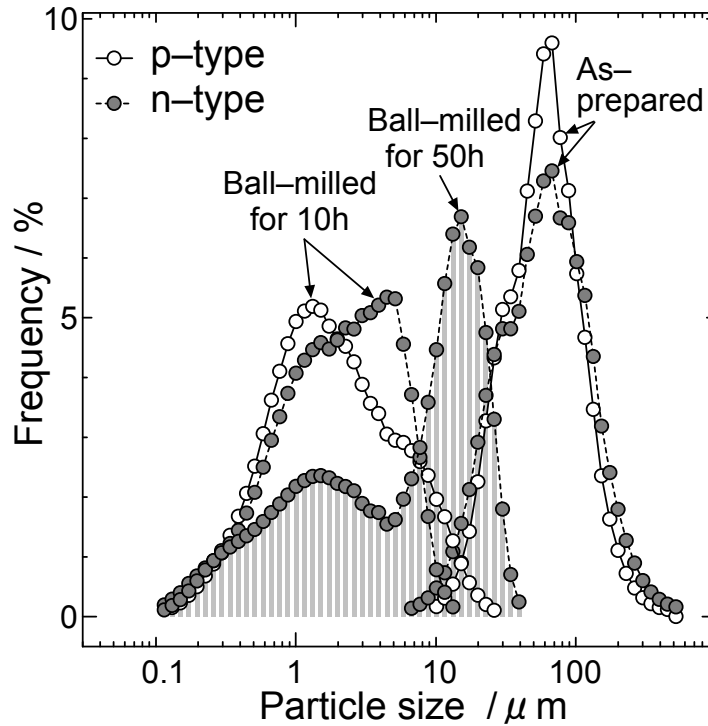


Fig. 2.4. Change of particle size distribution of as-prepared Si-Ge powders by ball-milling.

Table 2.2. Mean Particle Sizes of Si-Ge as-Prepared and their Pulverized Powders (μm)

	p-type Si-Ge	n-type Si-Ge
As-prepared	72.1	66.1
Pulverized 1h	-	4.6
5h	-	3.2
10h	3.0	2.6
30h	-	9.2
50h	-	8.9

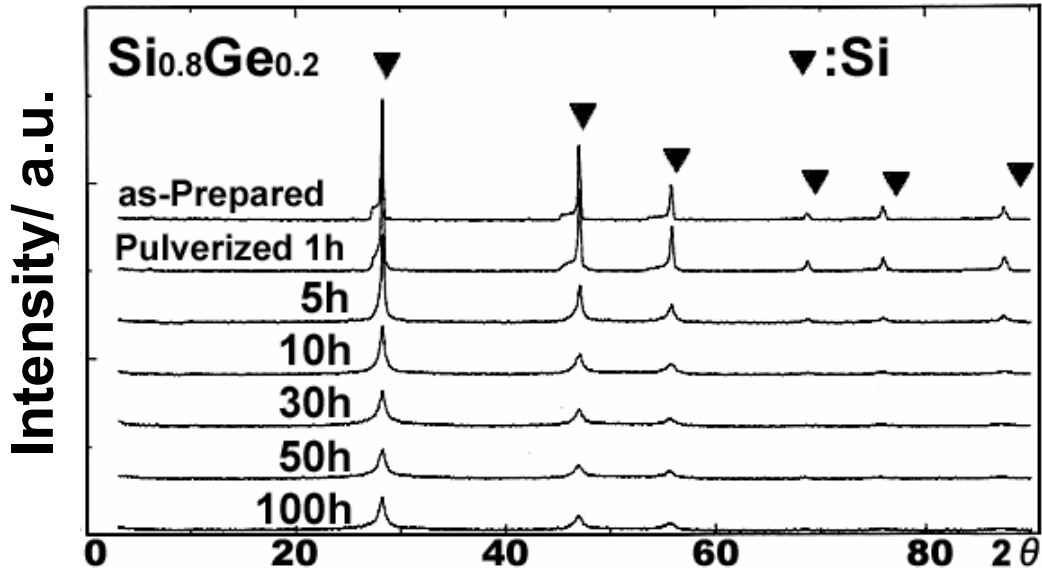


Fig. 2.5. XRD patterns of n-type as-prepared Si-Ge powder and its pulverized powders ball-milled for 1-100 h.

are located between those of Si and Ge. The XRD pattern indicated as-prepared powder to be in the fairly well-crystallized state. The intensities and widths of the peaks respectively decreased and increased gradually with the ball-milling time, which is probably due to the decrease in the crystallite size and the increase in the heterogeneous distortion in the particles, respectively. The XRD patterns of dense bodies that were made from these as-prepared and pulverized powders by the pulse-current sintering indicated well-crystallized $\text{Si}_{0.8}\text{Ge}_{0.2}$.

2.3.2 Densification

The densities of A_p and A_n increased abruptly at approximately 1500 K to reach the final stage of densification, as shown in **Fig. 2.6**. The densities were $2.56\text{-}2.64 \times 10^3 \text{ kg m}^{-3}$ at 1493 K, and became more than $2.88 \times 10^3 \text{ kg m}^{-3}$ above 1500 K. That is, a temperature above 1500 K was required for the complete densification of as-prepared powders. The density of P_p increased gradually until a temperature of 1393 K and then decreased, while

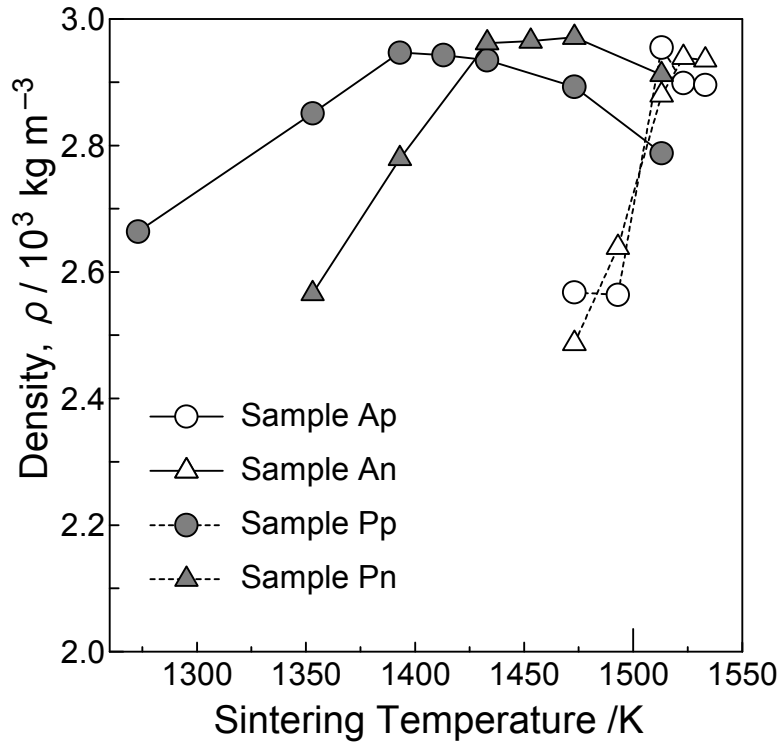


Fig. 2.6. Density of sintered bodies from p- and n-type as-prepared Si-Ge powders (A_p and A_n) and their pulverized powders ball-milled for 10 h (P_p and P_n).

that of P_n increased rather abruptly until 1433 K and started to decrease at over 1473 K.

In PCS process,, the actual temperature of the sample was higher than the measured temperature in the carbon vessel.¹³⁾ The local melting of contact points between the particles occurred to facilitate neck growth by overheating due to local concentration of the electric current.^{17), 18)} Consequently, the abrupt densification of as-prepared powders may be due to the liquefaction of small particles and the contact points between larger particles. The suitable sintering temperature range of these powders was limited within only 50 K because the melting point of $Si_{0.8}Ge_{0.2}$ was estimated to be 1550 K from the phase diagram of the Si-Ge system.¹⁶⁾ It was proved that the precise control of the sintering temperature was required to obtain a dense body from the powders.

On the other hand, the slow densification of pulverized powders occurred at a lower

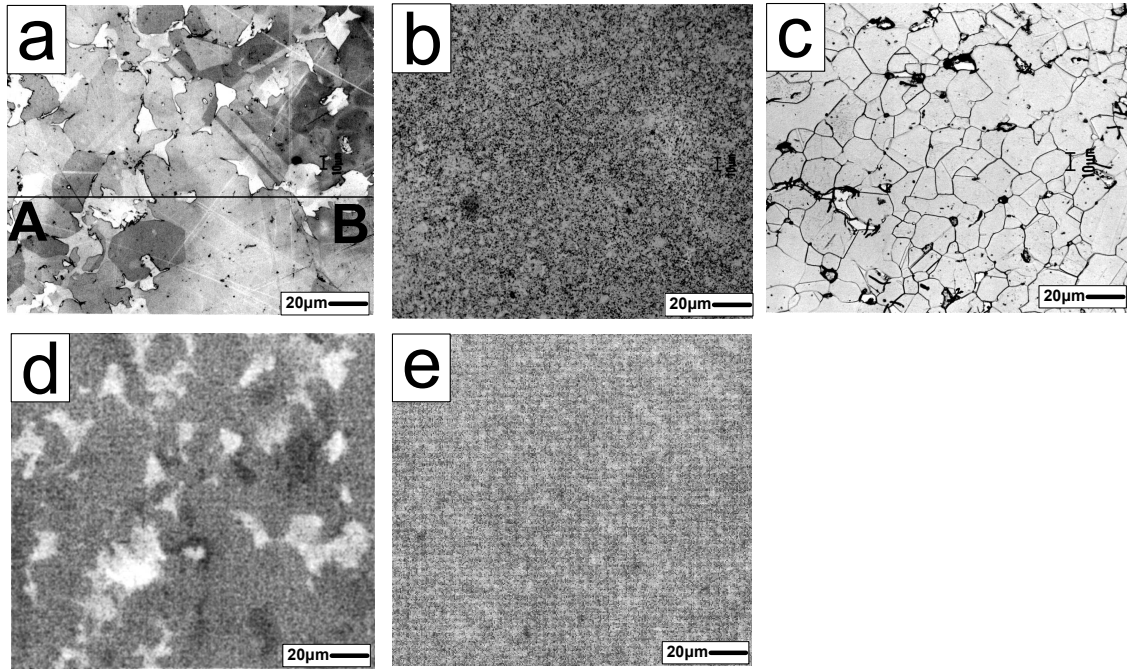


Fig. 2.7. Microstructures (a-c) and mapping image of Ge (d,e) of sintered bodies
 Microstructure of sintered bodies from (a) atomized Si-Ge powder,
 (b) pulverized Si-Ge powder and (c) atomized Si powder.

temperature compared with as-prepared powders. The suitable sintering temperature for sufficient densification was in the range between 1400 and 1450 K, which is much lower than the above estimated melting point of 1550 K. The densification then seemed to proceed by solid-state sintering. The difference of the density between P_p and P_n increased with decreasing temperature, depending on the size distribution rather than the mean particle size. **Table 2.2** shows almost the same particle size between two kinds of pulverized Si-Ge powders ball-milled for 10 h, but **Figure 2.4** shows that the frequency less than 2 μm of p-type pulverized powder surpasses that of n-type. The unexpected decreases in the densities of P_p and P_n above 1433 and 1473 K, respectively, were presumably attributed to an expansion of the microcrack inside the body accompanied by the evaporation of Ge that was supported by compositional analysis using X-ray fluorescence spectrometry. The surface activation of pulverized powders due to the introduction of the distortion may promote the evaporation of Ge from P_p and P_n . Sinterability of as-prepared p- and n-type

Si-Ge powders was confirmedly improved with the mechanochemically increased surface energy of the powders by ball-milling.

Oxygen of 1.0-1.2 mass% was contained in P_p and P_n as SiO_2 and/or GeO_2 , which was 20 times more than those of A_p and A_n . PCS was not interrupted by the surface oxide layers of the particles; the current passed through the shaped body without any interruption.^{17), 18)} However, the above-mentioned effect of the reduction of the grain size surpassed that of the contamination on the sinterability of P_p and P_n .

In comparison with the conventional hot pressing method, the densification and grain growth in this study were both similar^{7), 21)} but the working time of 180 s was remarkably short.

2.3.3 Microstructure and element distribution of sintered bodies

No microstructural difference was recognized between the p- and n-type of samples A and P observed in the optical micrographs. The microstructures of samples A_p , P_p and p-type Si from the corresponding gas-atomized powders are shown in micrographs in **Figs. 2.7(a)-(c)**. For sample A, many irregularly shaped areas 10-40 μm in length in light gray were observed in the matrix in dark gray (**Fig. 2.7(a)**). **Figure 2.7(b)** shows sample P consisting of many fine particles less than 5 μm in size. The grain boundaries were observed most clearly in the sample of pure Si, as shown in **Fig. 2.7(c)**, the grain size of which was almost the same as that of sample A.

Figures 2.7(d) and (e) are the mapping images of Ge of the samples A and P, corresponding to **Figs. 2.7(a) and (b)**, respectively. **Figure 2.7(d)** revealed that the light gray areas in **Fig. 2.7(a)** were rich in Ge. Further analysis of the Si and Ge distributions along the line from A to B in **Fig. 2.7(a)** was carried out, as shown in **Fig. 2.8**. The inhomogeneity of the Ge distribution of as-prepared Si-Ge powder surface shown in **Fig. 2.1** has been maintained in sample A, presumably due to a short time of 180 s for the pulse current sintering. The area ratio of the Si-rich (dark gray) and Ge-rich (light gray) phases in

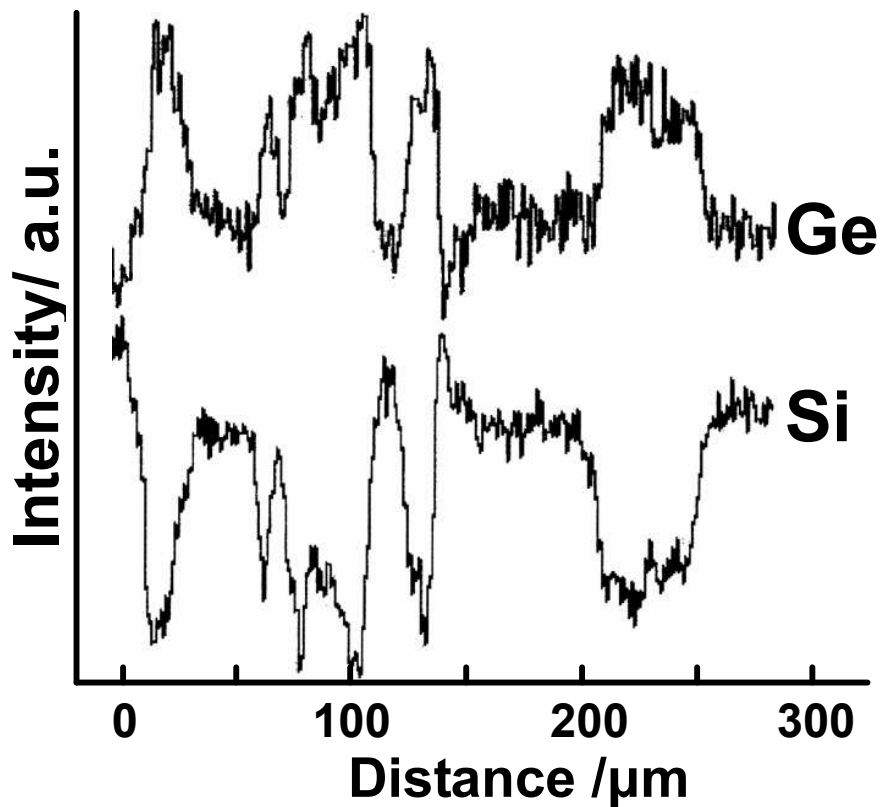


Fig. 2.8. Elemental distributions of Si and Ge along the line A-B in Fig. 2.7 (a).

Fig. 2.7(d) was determined to be 0.79 to 0.21 by conventional picture processing. Using the phase diagram of the Si-Ge system, this ratio gave an apparent temperature of 1585 K for solidification, followed by the determination of the compositions of 85Si-15Ge (mass%), and 61Si-39Ge of the dark and light gray areas, respectively. Finally, **Fig. 2.7(e)** shows that the inhomogeneity of sample P was improved compared with that of sample A.

2.3.4 Morphology of sintered bodies

The SEM images of the fracture surfaces of samples A and P show the relationship between the sintering temperature and the microstructure of the dense bodies. Many micropores 10-50 μm in length were observed in A_p sintered at 1493 K (**Fig. 2.9(a)**), indicating the insufficient densification. The considerable densification of A_p occurred in

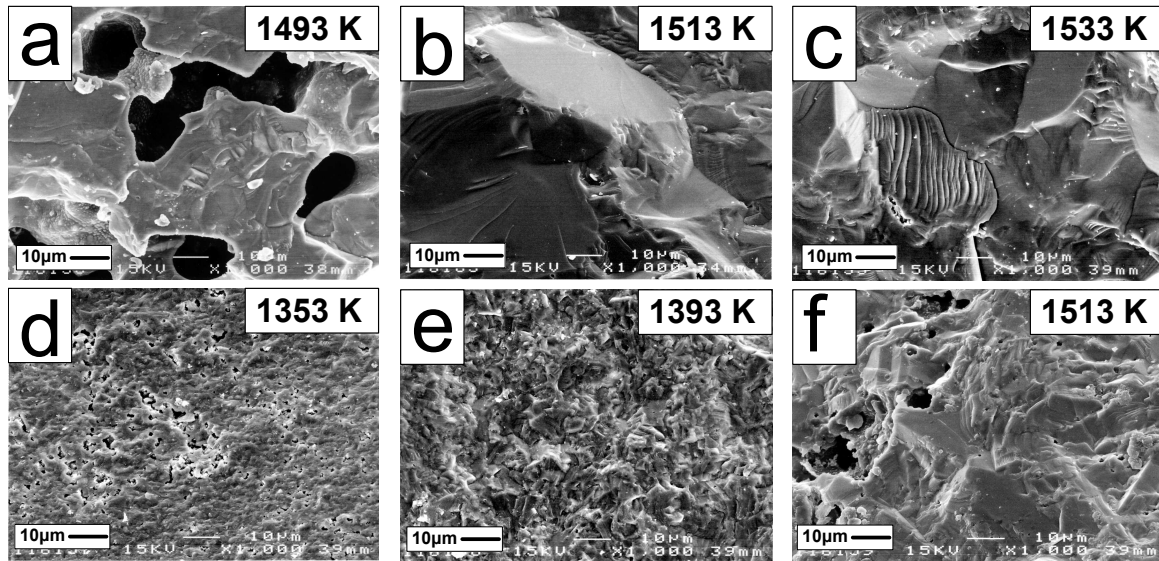


Fig. 2.9. Fracture surfaces of compact bodies from as-prepared Si-Ge powder sintered at (a) 1493 K, (b) 1513 K and (c) 1533 K, and from its pulverized powder sintered at (d) 1353 K, (e) 1393 K and (f) 1513 K.

the narrow temperature range between 1493 and 1513 K. The pores disappeared completely above 1513 K (**Figs. 2.9(b) and (c)**), having rough fracture surfaces. While fine pores less than 2 μm in size were observed in P_p sintered at 1353 K (**Fig. 2.9(d)**), they disappeared at 1393 K (**Fig. 2.9(e)**). These fracture surfaces of P_p sintered at 1353 and 1393 K consisted of small grains without growth. **Figure 2.9(f)** shows the abrupt increase in the grain size and the regeneration of some pores in P_p at 1513 K. Particularly, the latter implies the formation of microcracks inside the body due to the evaporation of Ge. The enhancement of the sinterability of as-prepared powder pulverized by ball-milling was confirmed from the comparison between the fracture surfaces of A_p and P_p sintered at 1513 K and 1393 K (**Figs. 2.9(b) and (e)**), respectively. This finding was also supported by the difference in the transverse rupture strengths of A_p and P_p (**Figs. 2.9(b) and (e)**) of the same density of almost 100 %, which were 118 and 161 MPa, respectively.

2.4 Summary

Both p- and n-type $\text{Si}_{0.8}\text{Ge}_{0.2}$ powders (Si: Ge: B = 79.7: 20.1: 0.21 mol% for p-type and 79.8: 20.0: 0.18 mol% for n-type) oriented to the thermoelectric element were prepared by gas atomization of the corresponding melts, followed by densification using a pulse-current sintering technique. These Si-Ge powders were characterized and their sinterability was then studied. The effect of ball-milling on the sinterability of the powders was also discussed. The composition of as-prepared n-type Si-Ge powder was different from the batch compositions due to melting and evaporation of the dopant at a high temperature. The mean particle sizes of as-prepared p- and n-type Si-Ge powders were 72 and 66 μm , respectively. The mean particle sizes of both types of as-prepared powders were shifted to 3.0 and 2.6 μm by ball-milling for 10 h, respectively. The decrease in the crystallite size and the increase in the heterogeneous distortion in the particles correlated with the ball-milling time. The densification of as-prepared powders was abruptly promoted above 1500 K; however, the densification temperature of the ball-milled powders decreased by approximately 100 K. That is, the sinterability of as-prepared powders was improved with the decrease in the crystallite size and the increased surface distortion mechanochemically introduced by ball-milling. The grain size and elemental inhomogeneity of the dense bodies were both reduced.

References

- 1) Vining, C. and Fleurial, J. P., "Silicon Germanium, An overview of recent developments," ed. by Rowe, D. M., Babrow Press, Cardiff, United Kingdom (1991), pp.1-14.
- 2) Scoville, N., Bajgar, C., Rolfe, J., Fleurial, J. P. and Vandersande, J., Proc. 28th Intersociety Energy Conversion Engineering Conference, pp.1227-1233 (1993).
- 3) Fleurial, J. P., Borshchevsky, A. and Vandersande, J. W., AIP Conference Proceedings, pp.451-457 (1991).
- 4) Scoville, N., Bajgar, C., Vandersande, J. and Fleurial, J. P., Proc. 27th Intersociety

- Energy Conversion Engineering Conference, pp.3465-3470 (1992).
- 5) Vining, C. B., Laskow, W., Hanson, J. O., Beck, R. R. and Gorsuch, P. D., *J. Appl. Phys.*, Vol.**69**, pp.4333-4340 (1991).
 - 6) Beaty, J. S., Rolfe, J. L. and Vandersande, J., American Institute of Physics Conference Proceedings, pp446-450 (1991).
 - 7) Beaty, J. S., Rolfe, J. L., Vandersande, J. and Fleurial, J. P., Proc. 27th Intersociety Energy Conversion Engineering Conference, pp.3471-3475 (1992).
 - 8) Lowley, A., *J. Metals*, Vol.**33**, pp.1-13 (1981).
 - 9) Lubanska, H., *J. Metals*, Vol.**22**, pp.45-49 (1970).
 - 10) Helmersson, G., Hede, A., Johannesson, T., Bergman, B., Hallen, H. and Burgdorf, K., “Advances in Powder Metallurgy & Particulate Materials-1996”, ed. by Terry Cadle and K S Narasimhan, Metal Powder Industries Federation, Princeton New Jersey, USA (1996) pp.1-109-1-124.
 - 11) Miller, S. A., Feingold, E. and Vining, C. B., *Modern Developments in Powder Metallurgy*, Vol.**17**, pp.671-682 (1985).
 - 12) Omori, M., *Mater. Sci. Eng.*, Vol.**A287**, pp.183-188 (2000).
 - 13) Kim, H. T., Kawahara, M. and Tokita, M., *Powd. Metall.*, Vol.**47**, pp.887-891 (2000).
 - 14) Wang, S. W., Chen, L. D. and Hirai, T., *J. Mater. Res.*, Vol.**15**, pp.982-987 (2000).
 - 15) Noguchi, T., Proc. 16th Int. Conf. on Thermoelectrics, pp207-214 (1997).
 - 16) Nihon Kinzoku Gakkai ed., Kinzoku Data Book 3rd ed., p.545 (1993).
 - 17) Nagae, T., Yokota, M., Nose, M., Tomida, S., Kamiya, T. and Saji, S., *Mater. Trans.*, Vol.**43**, pp.1390-1397 (2002).
 - 18) Murayama, N., *Ceramics Japan*, Vol.**32**, pp.445-449 (1997). [in Japanese]
 - 19) Rowe, D. M. and Shukla, V. S., *J. Appl. Phys.*, Vol.**52**, pp.7421-7426 (1981).

Chapter 3 Thermoelectric Properties of Si-Ge Dense Body

3.1 Introduction

Many efforts were devoted to enhance the thermoelectric properties of Si-Ge dense bodies.¹⁾ Fleurial et al.²⁾ and Scoville et al.^{3),4)} attempted to improve the thermoelectric properties of GaP-doped n-type Si-Ge by controlling carrier concentration and mobility. Scoville et al.⁴⁾ and Beaty et al.^{5),6)} enhanced those of p-type Si-Ge by reducing thermal conductivity through the addition of BN powder.

In the previous chapter, we found that ball-milling enhanced the sinterability of gas-atomized Si-Ge powders owing to the reduction of grain size and the introduction of surface strain energy. It was expected that ball-milling would also affect the thermoelectric properties of the dense bodies. In this chapter, the Seebeck coefficient, electrical resistivity and thermal conductivity of Si-Ge dense bodies that were prepared by PCS of the corresponding gas-atomized powders were determined to clarify the effect of the sample preparation methods, particularly paying attention to the grain size reduction by ball-milling.

3.2 Experimental

3.2.1 Sample preparation

Both p- and n-type Si-Ge powders were prepared by a gas-atomizing method,⁷⁾ as described in a previous chapter. The chemical compositions of as-prepared powders were Si 79.7 mol%, Ge 20.1 mol% and B 0.20 mol% for p-type, and Si 79.8 mol%, Ge 20.0 mol% and P 0.20 mol% for n-type. The mixing ratio of Si and Ge was determined to be 80:20 in mol% according to the report of Vining.¹⁾ A part of the gas-atomized powders was further pulverized by ball-milling at 400 rpm for 10 h in argon. The densification of as-prepared or further pulverized powders was carried out using a PCS apparatus⁸⁾ (Sumitomo Coal Mining Co., SPS-1030). A powder sample of 3 g was placed in a cylindrical carbon vessel

with an inner diameter of 20 mm and then uniaxially compressed with a carbon punch at 49 MPa. Sintering was carried out to fabricate a compact for a soaking time of 180 s in vacuo, providing the pulse current through the punch. The sintering temperatures of as-atomized and pulverized powders were 1523 and 1433 K, respectively. The low sintering temperature of the pulverized powders was due to the mechanochemically increased surface energy by ball-milling. The carbon vessel was enclosed inside a carbon thermal insulator to realize temperature uniformity of the charged powder. The sintering temperature was measured with a Pt-(Pt-13%Rh) thermocouple inserted into the vessel wall adjacent to the sample. Sintered bodies from p-type and n-type as-prepared powders were labeled A_p and A_n , respectively, and those from pulverized powders, P_p and P_n , respectively.

3.2.2 Characterization

A rectangular sample of 3 mm × 3 mm × 15 mm size was cut from a sintered body of 20 mm diameter and 4 mm thickness, and fixed between high- and low-temperature parts in a sample holder of a thermoelectric measurement apparatus (ULVAC-RIKO, ZEM-1), as



Fig. 3.1. Appearance of thermoelectric measurement apparatus.

shown in **Fig. 3.1**, Sample was brought into contact with a pair of probes for the measurement of both voltage and temperature, which were 10 mm apart. Seebeck coefficient and electric resistivity were simultaneously measured from room temperature to 1073 K in He with the temperature differences of 20, 30 and 40 K between the two probes.

Thermal diffusivity α (cm^2s^{-1}) and specific heat C_p ($\text{Jg}^{-1}\text{K}^{-1}$) were measured in vacuo from room temperature to 1073 K with a laser flash thermal constant analyzer (ULVAC-RIKO, TC-7000) using a disk sample of 10 mm diameter and 2 mm thickness which was cut from the above sintered body. One side of the sample was heated with a ruby laser flash, and the temperature of the back surface was measured with a thermocouple or infrared detector. Specific heat was calibrated with a sapphire sample. Then, thermal conductivity κ is obtained by multiplication of α , C_p and density. The κ is given by the sum of lattice thermal conductivity (κ_{ph}) and electronic thermal conductivity (κ_{el}) as follows:⁹⁾

$$\kappa = \kappa_{ph} + \kappa_{el}. \quad (3.1)$$

According to the Wiedemann-Frantz law, κ_{el} can be expressed as

$$\kappa_{el} = LT / \rho, \quad (3.2)$$

where L is the Lorentz number and T is the absolute temperature. The κ_{ph} of the sample was calculated using equations (1) and (2). Here, the Lorentz number, $L=2.44 \times 10^{-8} \text{ W}\Omega\text{K}^{-2}$ of $\text{Si}_{0.78}\text{Ge}_{0.22}$ determined at low temperatures¹⁰⁾ was used. The oxygen content of both the powder and sintered body was determined by measuring the amount of carbon dioxide generated from the melted sample in a carbon crucible using an oxygen/nitrogen analyzer (HORIBA, EMGA-620W).

3.3 Results and discussion

3.3.1 Thermoelectric properties

A_p and A_n had the density of 99.6%, and P_p and P_n had that of 100%; the former included large grains more than 20 μm in size, and the latter consisted of small grains less than 5 μm in size, as seen in previous chapter. The XRD patterns of these sintered bodies all

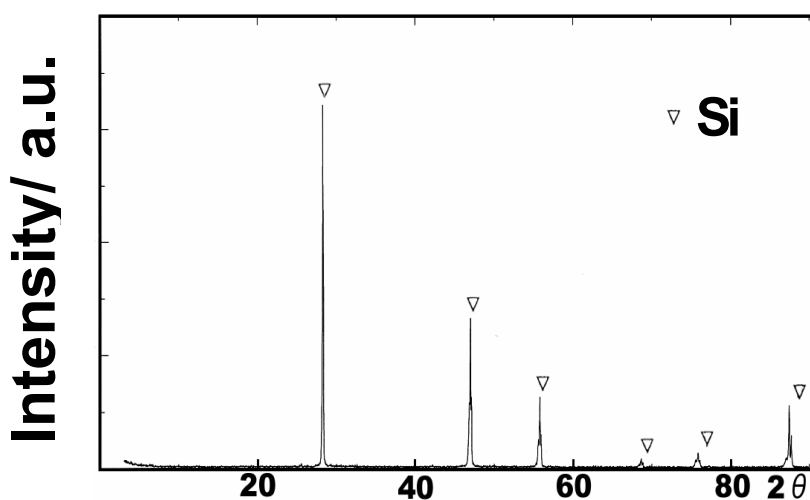


Fig. 3.2. A typical XRD pattern of $\text{Si}_{0.2}\text{Ge}_{0.8}$ sintered body by pulse current sintering.

Sample: Sintered body from gas-atomized p-type powder (A_p)

indicated a well-crystallized Si-Ge single phase (**Fig. 3.2**).

The temperature dependences of lattice thermal conductivity, electric resistivity and Seebeck coefficient of p-type sintered bodies (A_p and P_p) are shown in **Fig. 3.3**. It is well known that the thermal conductivity of a thermoelectric material decreases with decreasing grain size.^{11),12)} In this study, the lattice thermal conductivity of P_p , consisted of small grains as mentioned above, was smaller than that of A_p in the temperature range of 300-1073 K except 673 K, as shown in **Fig. 3.3(a)**, which seems to be attributed to an increase in phonon scattering at the grain boundary.^{13),14)}

The Seebeck coefficients of A_p and P_p monotonically increased with temperature, as shown in **Fig. 3.3(b)**. No significant difference between A_p and P_p was observed, indicating the independence from the grain size. Slack and Hussain theoretically suggested that Seebeck coefficient is affected by grain size only when the grain size is less than $0.01 \mu\text{m}$ of the electron mean-free path.¹⁵⁾ **Figure 3.3(c)** shows that the resistivities of A_p and P_p increased linearly with temperature. The resistivity of P_p was higher than that of A_p in the entire temperature range considered, probably due to the difference in grain size. Electrical

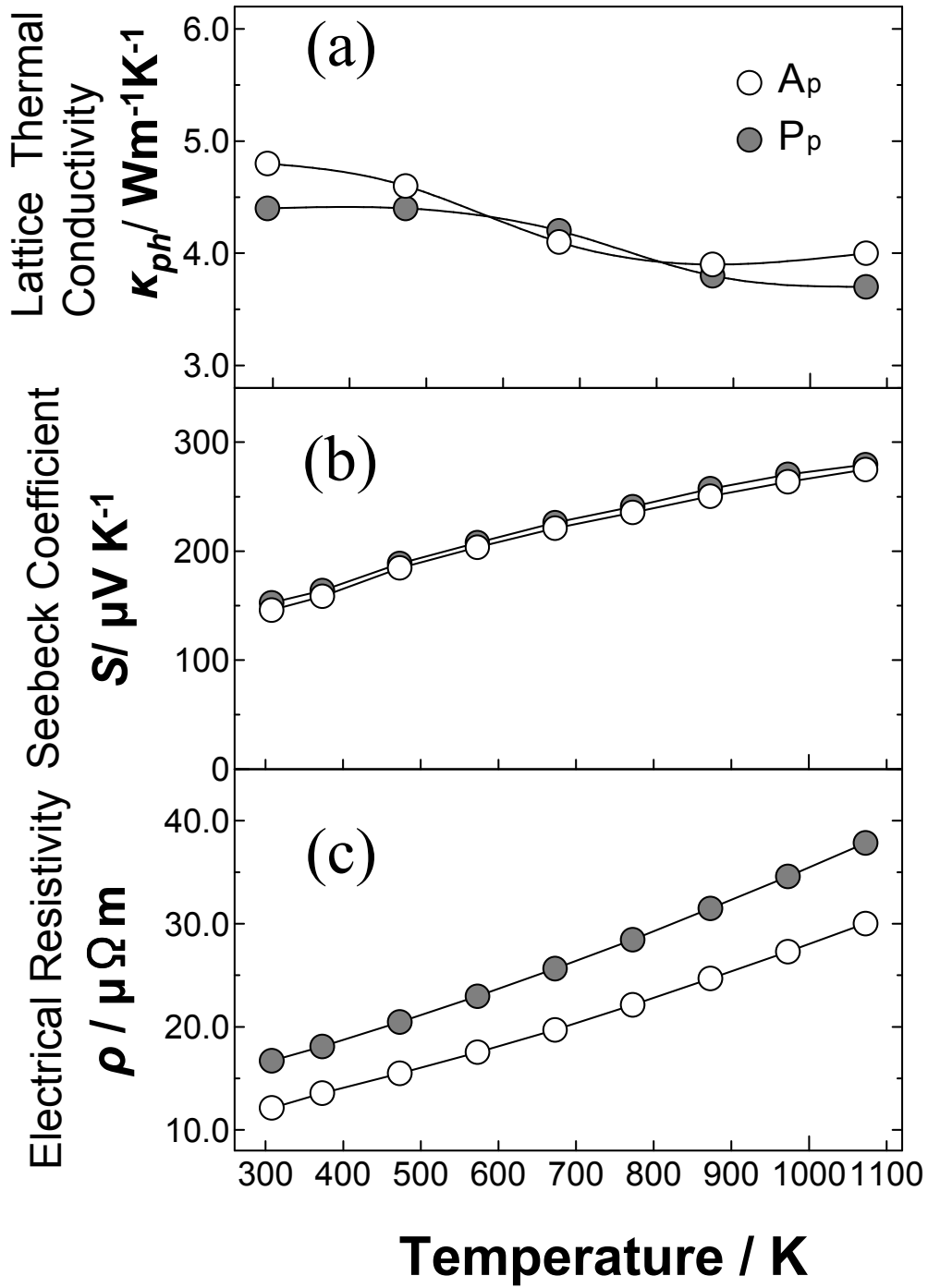


Fig. 3.3. Thermoelectric parameters of Si-Ge sintered bodies from as-prepared and its pulverized p-type powders (A_p and P_p).

conductivity σ is expressed as

$$\sigma = 1/\rho = n e \mu, \quad (3.3)$$

where n , e and μ denote the concentration, charge and mobility of charge carriers, respectively. The carrier concentration of P_p appeared to be the same as that of A_p , judging from the result that these samples had the same Seebeck coefficient (**Fig. 3.3(b)**). Therefore, the higher resistivity of P_p than that of A_p may be attributed to the decrease in the mobility of the charge carriers caused by the fine-grained structure. This increase in the electrical resistivity indicates that the thermal conductivity was reduced by the decrease in both κ_{ph} and κ_{el} .

The thermoelectric parameters of n-type Si-Ge sintered bodies are also shown in **Fig. 3.4**. There was no significant difference in the temperature dependences of these parameters between those of p- and n-type samples. As in the case of p-type, P_n have a lower thermal conductivity and higher resistivity than A_n probably due to the fine-grained structure. However, the Seebeck coefficient of P_n was slightly lower than that of A_n (**Fig. 3.4(b)**), and the difference in resistivity between P_n and A_n was smaller than that of p-type (**Fig. 3.4(c)**). As carrier concentration increases, electrical conductivity increases proportionally while Seebeck coefficient decreases logarithmically.⁹⁾ Thus, the slight enhancement of the carrier concentration of P_n possibly occurred through ball-milling, followed by the slight decrease in the resistivity and the Seebeck coefficient of the sample.

The thermal conductivities of P_p and P_n were 8 and 10% lower on average in the temperature range of 300-1073 K than those of A_p and A_n , respectively, as shown in **Figs. 3.3(a)** and **3.4(a)**. The specific heat of P_p was found to be slightly higher than that of A_p , although it is known to be insensitive to the microstructure of the material (**Table 3.1**).¹⁶⁾ The thermal diffusivity of P_p was lower than that of A_p . The n-type Si-Ge also had the same tendency of specific heat and thermal diffusivity as the p-type. These results indicated that the decreases in the thermal conductivities of P_p and P_n by ball-milling were attributed to the decrease in their thermal diffusivities.

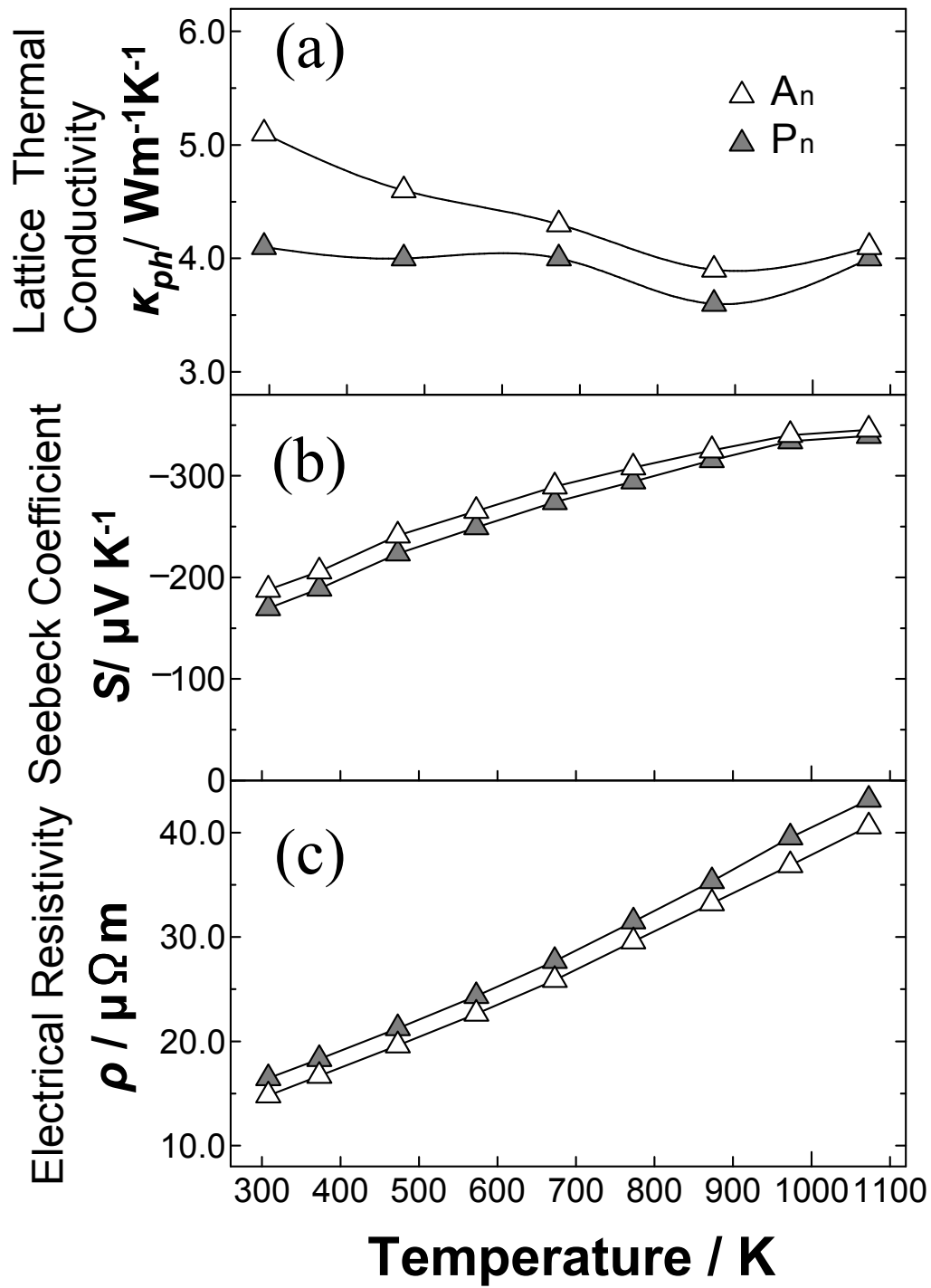


Fig. 3.4. Thermoelectric parameters of Si-Ge sintered bodies from as-prepared and its pulverized n-type powders (A_n and P_n).

Table 3.1. Specific Heat, Thermal Diffusivity and Thermal Conductivity (at 873 K)

		p-type		n-type	
		A _p	P _p	A _n	P _n
Specific Heat	C _p / Jg ⁻¹ K ⁻¹	0.74	0.78	0.72	0.74
Thermal Diffusivity	α / cm ² s ⁻¹	0.022	0.019	0.022	0.019
Thermal Conductivity	κ / Wm ⁻¹ K ⁻¹	4.8	4.4	4.5	4.2

3.3.2 Figure of merit

The conversion efficiency from heat to electrical energy in a thermoelectric generator depends on the thermoelectric figure of merit which is determined by⁹⁾

$$ZT = S^2 T / \rho \kappa, \quad (3.4)$$

where ZT is dimensionless figure of merit, S Seebeck coefficient (VK⁻¹), ρ resistivity (Ω m) and κ thermal conductivity (Wm⁻¹K⁻¹). **Figure 3.5** shows that the ZT of n-type Si-Ge exceeded that of p-type, which was based on the difference in Seebeck coefficient, as shown in **Figs. 3.3(b)** and **3.4(b)**. The ZT of A_p and P_p increased monotonically from 300 to 1073 K, but the value of P_p was lower than that of A_p in this temperature range. Those of A_n and P_n increased monotonically from 300 to 873 K and the slopes of the lines of these samples slightly decreased above 873 K due to the slight increase in thermal conductivities (**Fig. 3.4(a)**). The lowering of the ZT of P_n compared to that of A_n was also observed from 300 to 873 K.

The differences in ZT between Si-Ge dense bodies sintered with as-prepared and pulverized powders were 13% in p-type and 8% in n-type, respectively, in the temperature range of 300-1073 K. A_p and A_n displayed better thermoelectric abilities than P_p and P_n since the effect of the decrease in resistivity exceeded that of the increase in thermal conductivity, according to equation (3.3). Vining et al. also reported that the thermal

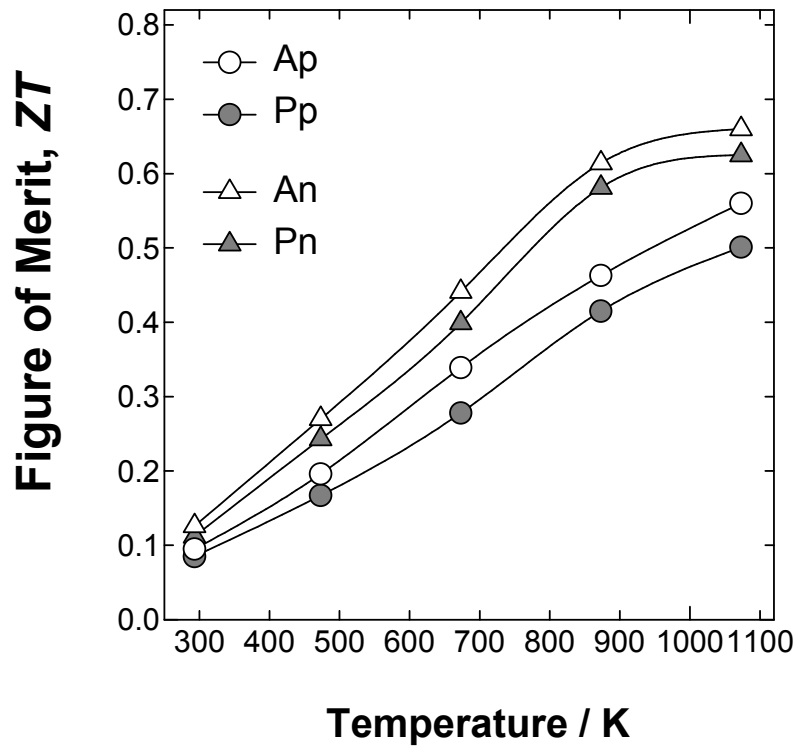


Fig. 3.5. Figure of merit ZT of Si-Ge sintered bodies from as-prepared and its pulverized powder.

conductivity of the Si-Ge sintered body from powders with various grain sizes ranging from 1 to 100 μm decreased with decreasing grain size; however, the figure of merit did not significantly increase due to a compensating reduction in electrical conductivity.¹⁶⁾ In this study, the thermoelectric properties were not improved by the reduction in the grain size of the Si-Ge sintered body by ball-milling.

The oxygen contents of sintered bodies with their starting powders are shown in **Fig. 3.6**. The oxygen contents of P_p , P_n , and their powders were found to be approximately 20 times more than those of A_p , A_n , and their powders. The metal oxide, that is SiO_2 and GeO_2 , probably formed on the grain surface in air after ball-milling, and then the resistivity of P_p and P_n may have been enhanced by this metal oxide layer which existed at the grain boundary, as suggested by Slack and Hussain.¹⁵⁾ It was also observed that the oxygen

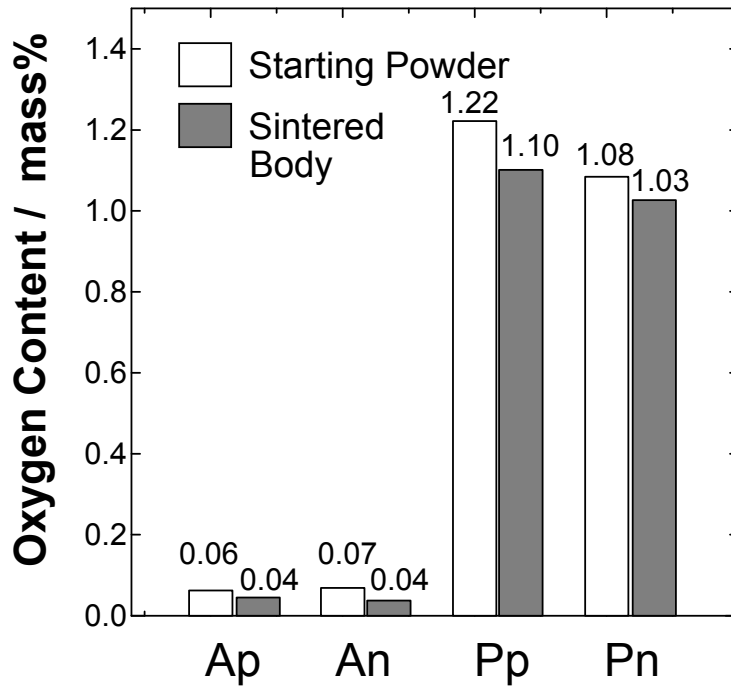


Fig. 3.6. Oxygen content of Si-Ge powders and their sintered bodies.

contents of all the sintered bodies were slightly lower than those of the corresponding starting powders, which was probably attributed to the reducing atmosphere of the PCS process due to the use of a carbon vessel in vacuo.

The ZT of A_p was higher than that of Noguchi's sample¹⁸⁾ from 300 to 1073 K, however, slightly lower than that of Vining's sample¹⁷⁾ above 700 K (**Fig. 3.7(a)**). The ZT of A_n was almost the same as that of Noguchi's sample but lower than that of Vining's sample above 500 K (**Fig. 3.7(b)**). The thermal conductivity, Seebeck coefficient and resistivity of p- and n-type $Si_{0.8}Ge_{0.2}$ sintered bodies at 873 K are summarized in **Table 3.2**. The Seebeck coefficient of n-type samples seems to strongly depend on dopant concentration, while resistivity seems to be affected by both dopant concentration and the microstructure. The resistivity of A_p was the lowest probably due to the large grain size and low oxygen content. Thus, the larger ZT of A_p than that of Noguchi's sample was attributed to the low resistivity of this sample, as shown in **Fig. 3.7(a)**, which may be caused by the powder preparation

method. The difference in thermal conductivity between this study and that of Noguchi was obscure, while the thermal conductivity of Vining’s samples was significantly lower than those of the other two samples. Thus, the ZT values of both Vining’s p- and n-type samples were relatively high.

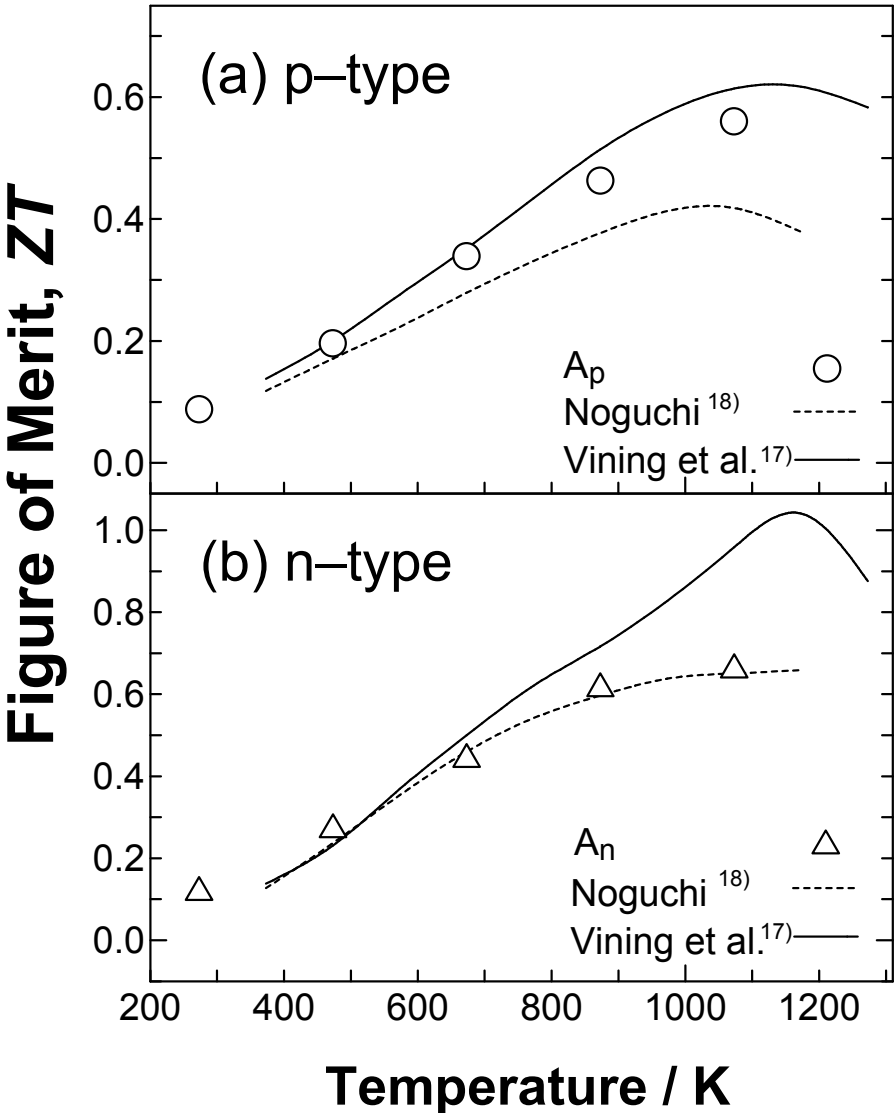


Fig. 3.7. Figure of merit ZT of (a) p-type and (b) n-type $\text{Si}_{0.8}\text{Ge}_{0.2}$ sintered bodies.

Table 3.2. Seebeck Coefficient, Resistivity, Thermal Conductivity of p- and n-type Si_{0.8}Ge_{0.2} (at 873K)

		Dopant /mol%	Powder	Sintering	κ /Wm ⁻¹ K ⁻¹	S / μ VK ⁻¹	ρ / μ Ω m
A _p	p-type	0.20B	Atomized	PCS	4.8	251	24.7
Noguchi ¹⁸⁾		0.20B	Pulverized	PCS	4.9	241	27.1
Vining et al. ¹⁷⁾		0.23B	Pulverized	Hot Pressing	3.6	236	25.7
A _n	n-type	0.20P	Atomized	PCS	4.5	-325	33.2
Noguchi ¹⁸⁾		0.30P	Pulverized	PCS	4.7	-292	25.9
Vining et al. ¹⁷⁾		0.59P	Pulverized	Hot Pressing	3.6	-267	23.0

3.4 Summary

The thermoelectric properties of p- and n-type Si_{0.8}Ge_{0.2} dense bodies formed by pulse-current sintering of their gas-atomized and pulverized powders by ball-milling were investigated in the temperature range from room temperature to 1073 K. The pulse-current sintering of the gas-atomized and pulverized powders possibly yielded the shaped bodies with a density of more than 99 % at 1523 and 1433 K, respectively, in a short time of 3min. The results obtained in this study were all attributed to the thermoelectric properties such as the thermal conductivity, electric resistivity and Seebeck coefficient of the dense bodies. It has been proved that the figure of merit of sample A_n was the highest among the four kinds of dense bodies tested and that further pulverization of the gas-atomized powders by ball-milling was ineffective. It was also found that the application of the gas-atomized powder for fabricating Si-Ge sintered body has the advantage of the reduction in oxygen content and resistivity compared to the case of the pulverized powders.

References

- 1) Vining, C. and Fleurial, J. P., "Silicon Germanium, An overview of recent developments," Ed. by Rowe, D. M., Babrow Press, Cardiff, United Kingdom (1991) pp.1-14.

- 2) Fleurial, J. P., Borshchevsky, A. and Vandersande, J. W., AIP Conference Proceedings, pp.451-457 (1991).
- 3) Scoville, N., Bajgar, C., Vandersande, J. and Fleurial, J. P., Proc. 27th Intersociety Energy Conversion Engineering Conference, pp.3465-3470 (1992).
- 4) Scoville, N., Bajgar, C., Rolfe, J., Fleurial, J. P. and Vandersande, J., Proc. 28th Intersociety Energy Conversion Engineering Conference, pp.1227-1233 (1993).
- 5) Beaty, J. S., Rolfe, J. L. and Vandersande, J., AIP Conference Proceedings, pp.446-450 (1991).
- 6) Beaty, J. S., Rolfe, J. L., Vandersande, J. and Fleurial, J. P., Proc. 27th Intersociety Energy Conversion Engineering Conference, pp.3471-3475 (1992).
- 7) Miller, S. A., Feingold, E. and Vining, C. B., *Modern Developments in Powder Metallurgy*, Vol.17, pp.671-682 (1985).
- 8) Kim, H. T., Kawahara, M. and Tokita, M., *Powder and Powder Metal.*, Vol.47, pp.887-891 (2000).
- 9) Wood, C., *Rep. Prog. Phys.*, Vol.51, pp.459-539 (1988).
- 10) Kumar, G. S., Vandersande, J. W., Klitsner, T., Pohl, R. O. and Slack, G. A., *Phys. Rev. B*, Vol.33, pp.2157-2162 (1985).
- 11) Kusano, D., Hori, Y., Izumi, K., Kajikawa, T. and Shida, K., *J. Jpn. Inst. Metals*, Vol.63, pp.1429-1434 (1999). [in Japanese]
- 12) Nishida, I., "Thermoelectrics, Principals and Applications," Ed. by Sakata, R., Realize, Tokyo (2001) pp.186-195. [in Japanese]
- 13) Rowe, D. M. and Shukla, V. S., *J. Appl. Phys.*, Vol.52, pp.7421-7426 (1981).
- 14) Rowe, D. M., Proc. 4th Int. Conf. on Thermoelectric Energy Conversion, pp.96-103 (1982).
- 15) Slack, G. A. and Hussain, M. A., *J. Appl. Phys.*, Vol.70, pp.2694-2718 (1991).
- 16) Kingery, W. D., Bowen, H. K. and Uhlmann, D. R., "Introduction to Ceramics 2nd Ed," John Wiley & Sons, Inc., New York (1976) pp.586-589.

- 17) Vining, C. B., Laskow, W., Hanson, J. O., Beck, R. R. and Gorsuch, P. D., *J. Appl. Phys.*, Vol.**69**, pp.4333-4340 (1991).
- 18) Noguchi, T., Proc. 16th Int. Conf. on Thermoelectrics, pp.207-214 (1997).

Chapter 4 p-n Joined Si-Ge Thermoelectric Element

4.1 Introduction

For the reduction of energy consumption and the sustainable global environment, research work on thermal-electrical energy conversion has increased resulting in the development of effective thermoelectric elements which make use of the temperature difference between both ends of body.^{1),2)} Silicon-germanium (Si-Ge), one of high-temperature thermoelectric materials used in a temperature range of 500-1000°C, was fabricated by sintering of p- or n-type semiconducting powders.³⁾ Each powder was generally prepared by pulverizing the corresponding ingot,⁴⁾ or by using an atomizing technique.^{5),6)} The densification of each powder was carried out by hot pressing or pulse-current sintering (PCS), of which the latter could yield a dense body in a short period.⁷⁾ We reported the thermoelectric properties of p- and n-type Si-Ge dense bodies fabricated by PCS of gas-atomized powders,⁸⁾ where both figures of merit ZT , increased monotonically with temperature until 1073 K, and became 0.56 and 0.66, respectively.

Thermoelectric element is usually fabricated by connecting each end of p- and n-type dense semiconductors with a metal plate.⁹⁾ as shown in **Fig. 4.1(a)**. However, FeSi₂ element was differently fabricated with the direct contact by simultaneous sintering and joining of the p- and n-type powders, , as shown in **Fig. 4.1(b)**.¹⁰⁾⁻¹³⁾ Here, the electrical separation between both dense bodies was achieved in three different ways: the fabrication of U-shaped element with the corresponding die,^{10),11)} the insertion of a slit of an insulator between the two dense bodies.^{12),13)} This direct joining technique was possibly applied to for the fabrication of Si-Ge¹⁴⁾ and Li_{0.025}Ni_{0.975}O–Bi_{0.4}Sr_{0.6}PbO₃¹⁵⁾ by making a slit after sintering. Of these three methods, the insertion of insulator must be most effective for both the strengthening of element and the simplification of manufacturing process.

The output of thermoelectric element was determined from the voltage and electric current at a low temperature end during the p-n joint was heated at a prescribed

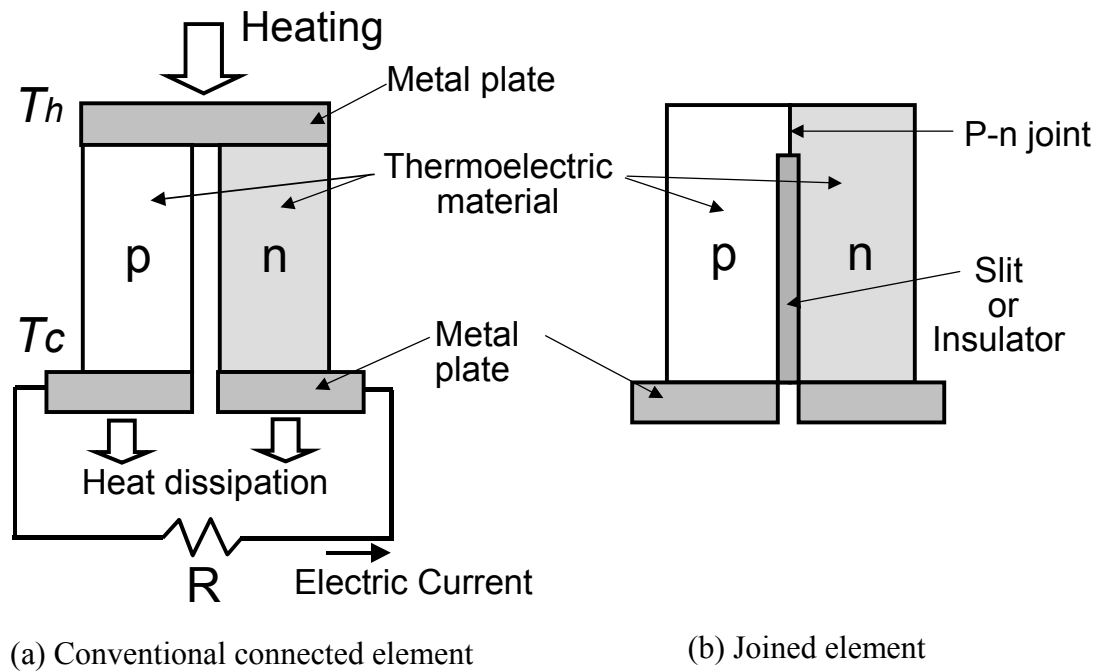


Fig. 4.1. Illustration of thermoelectric element.

temperatures with a hot plate or a furnace.¹⁴⁾⁻¹⁷⁾ That is, electric current, voltage drop by a reference resistor, and open circuit voltage of element were measured. The shape and size desirable for a high-efficiency thermoelectric element were determined from the theoretical analysis by the optimization of the length¹⁸⁾ or the ratio of the length and the cross sectional area¹⁹⁾ of the element. El-Genk et al. also discussed theoretically the output of connected GaP-added Si-Ge element under various external loads and heating conditions.²⁰⁾

In this paper, the fabrication of two types of p-n joined $\text{Si}_{0.8}\text{Ge}_{0.2}$ thermoelectric elements (hereafter, abbreviated as joined element) was attempted by PCS of gas-atomized p- and n-type Si-Ge powders. The relationship between the output and the dimensions of joined element was also discussed to determine preferable element configurations.

4.2 Experimental

4.2.1 Fabrication of joined element

The preparation procedure of joined element is shown in **Fig. 4.2**. Both p- and n-type Si-Ge powders were prepared by the gas atomization technique, as described in a

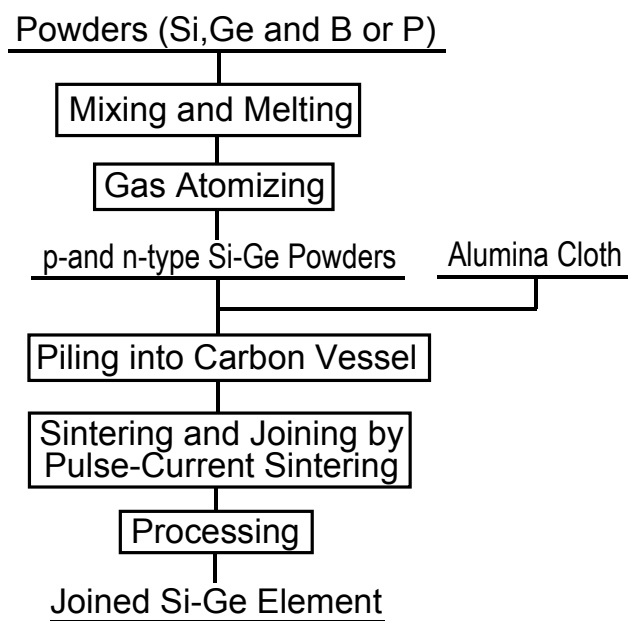


Fig.4.2. Flow diagram of preparation of joined element.

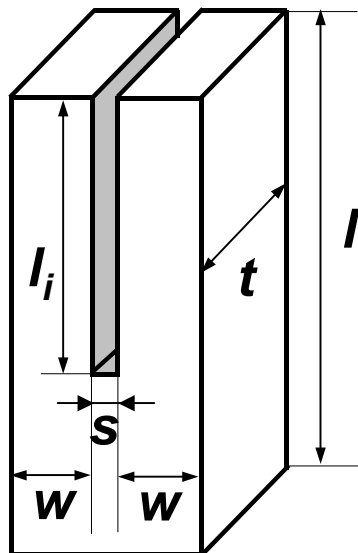


Table 4.1. Dimensions on the Configuration of Joined Si-Ge Elements (mm)

Sample	l	l_i	w
No.1	30	15	2.8
No.2	30	23	2.8
No.3	24	15	2.8
No.4	24	18	2.8
No.5	26	23.5	2.5

$t = 5.5 \text{ mm}, s = 0.5 \text{ mm}$

Fig. 4.3. Configurative parameters of joined element.

previous chapter.⁶⁾ The chemical compositions of p- and n-type powders obtained were Si 79.7 mol%, Ge 20.1 mol%, B 0.20 mol%, and Si 79.8 mol%, Ge 20.0 mol%, P 0.20 mol%, respectively. These powders of 7 g each were successively charged in a cylindrical carbon vessel with an inner diameter of 30 mm and then uniaxially compressed with a carbon punch at 49 MPa. The simultaneous sintering and joining were carried out by heating at 1523 K for a soaking time of 180 s in vacuo using a PCS apparatus (Sumitomo Coal Mining SPS-1030). As-sintered body was 30 mm in diameter and 7 mm in thickness, and it was further processed into a π -shaped joined element with a cutting machine, while, a slit was inserted to directly between the p-n joined Si-Ge dense body by cutting partly the joint. The configurative parameters of joined elements after being shaped are shown in **Fig. 4.3**. The joined element with a slit was fabricated according to the dimensions on the configuration shown in **Table 4.1**. Alumina cloth of 30 mm in diameter and 2mm in thickness (NICHIAS No.5475, Japan) as an insulator was cut off partly for the direct contact of the p- and n-type powders, and then was sandwiched between the two powders by PCS.

4.2.2 Characterization and evaluation

SEM observation and atomic line analysis near alumina layer of joined element were carried out using a scanning electron microscope (JEOL, JSM-6300) and an electron-probe microanalyzer (SHIMADZU, EPMA8705), respectively. As shown in **Figs. 4.4** and **4.5**, a set of measurement system was composed of both heating controller and electrical measurement; the heating apparatus consisted of infrared furnace, power supply, and temperature controller, whilst the electrical measurement consisted of data logger, measuring controller, and electronic load device. The infrared furnace has a dimension of 300 mm \times 250 mm \times 249 mm in size with 12 infrared lamps (ULVAC, infrared gold image furnace, Pss1108) and was surrounded with five aluminum boards attached with water cooling system. The top board has a squared hole of 40 mm \times 60 mm in the center for inserting an element. Heating with the infrared lamps was controlled by programmable

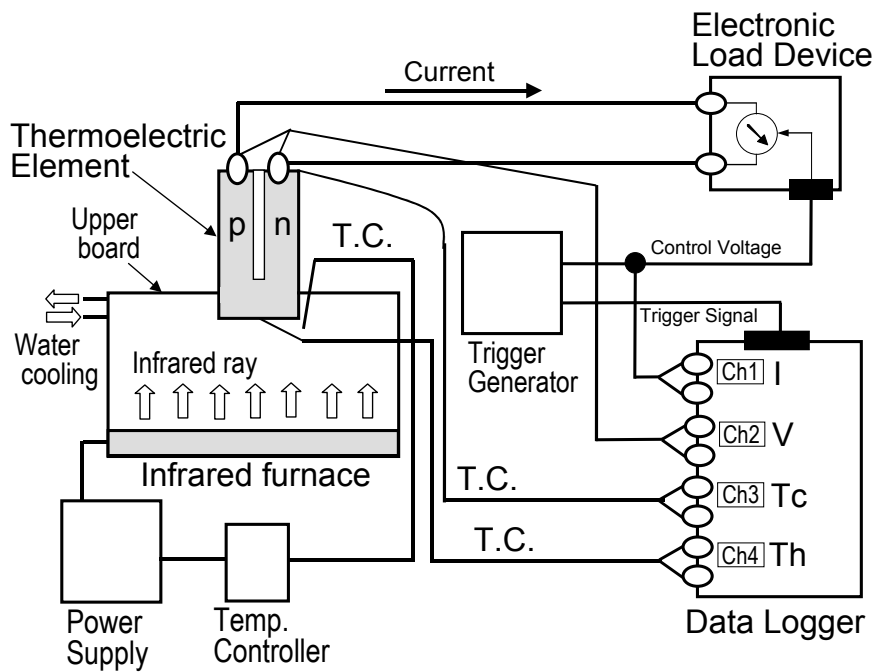


Fig. 4.4. Diagram of output measurement system for thermoelectric element.

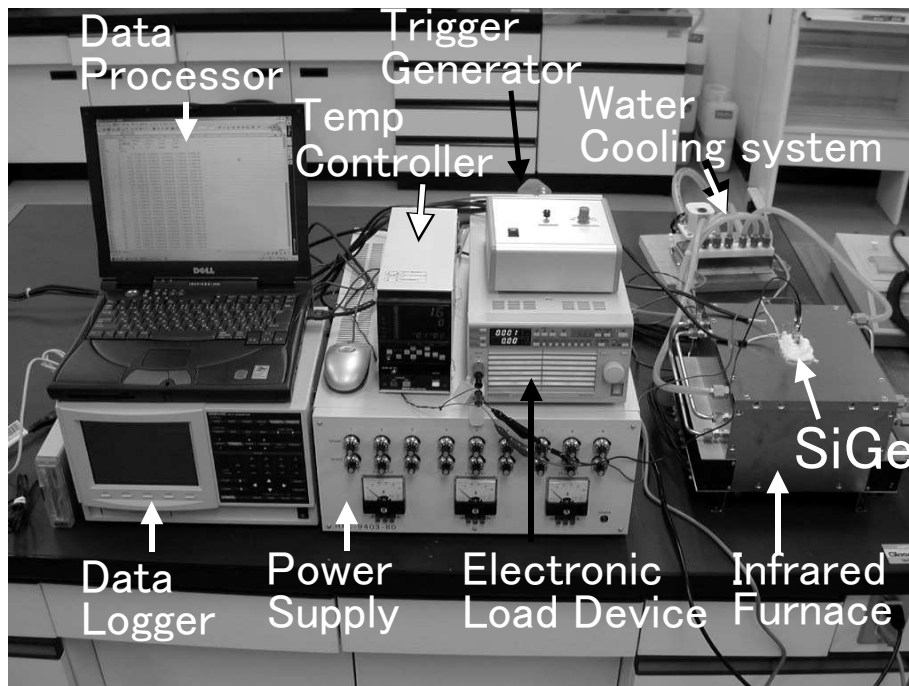


Fig. 4.5. Appearance of output measurement system.

temperature controller using a Pt-(Pt-13%Rh) thermocouple inserted into the furnace. The element was fixed at the above hole in top board with some insulator so that the p-n joint faced underside. Then the p-n joint of the element was heated at the prescribed temperatures ranging from room temperature to 1273 K. The voltage and electric current generated from the element were measured with data logger at each temperature. The temperatures at hot and cold ends of the element were also detected by using Pt-(Pt-13%Rh) thermocouples. After a starting signal was sent from a trigger generator, voltage (V), electric current (I), and temperatures at hot and cold ends of the element (T_h and T_c , respectively) were monitored by the data logger while the electric current through the element was controlled from 0 to 1.0 A by an electronic load device in 5 s. The temperature at the bottom of the slit of joined element, T_h' was estimated from the following equation:

$$T_h' = T_h - ((I - I_i)/I) (T_h - T_c). \quad (4.1)$$

The temperature difference, ΔT was calculated by $T_h' - T_c$. The electrical resistivity of the element was obtained from the slope of the voltage and electric current curve by using least square method. For the evaluation of the element the maximum output, (P_{max}) was calculated as the maximum value of the multiplication of voltage and electric current.

4.3 Results and discussion

4.3.1 Joined element

As shown in **Fig. 4.6**, both p-n joints of these elements formed via the PCS process were firmly connected without any crack as expected, because the thermal expansion coefficient of both types of Si-Ge were almost the same.²¹⁾ The alumina layer inserted between both gray Si-Ge dense bodies looked blackish. This joined element with alumina layer probably shows higher strength than the slit-introduced Si-Ge joined element. **Figure 4.7** shows that this layer of approximately 80 μm in width was composed of granular structure, and that no space or crack in the interfaces between alumina layer and joined element was observed in spite of the large difference of the thermal expansion coefficients

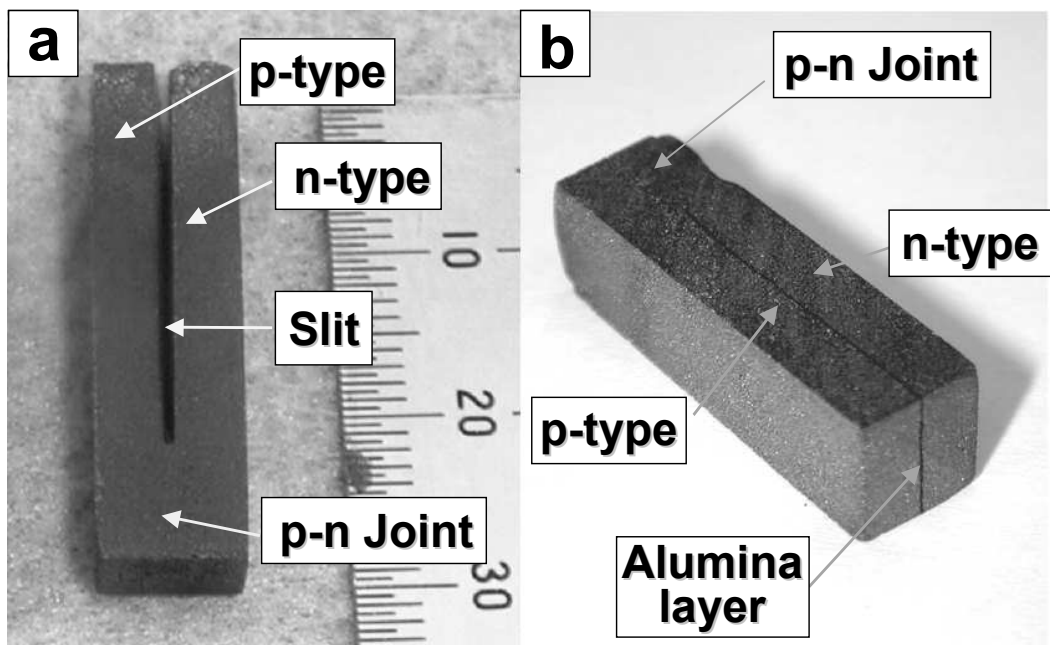


Fig. 4.6. Appearances of joined elements with a slit (a) and with an alumina layer (b).

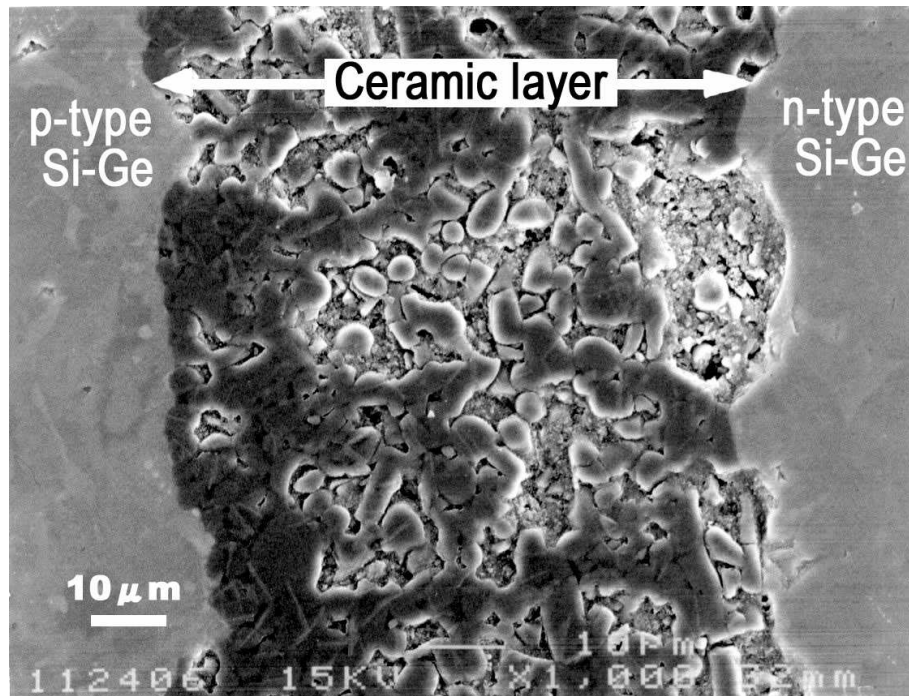


Fig. 4.7. SEM image of alumina layer of joined element.

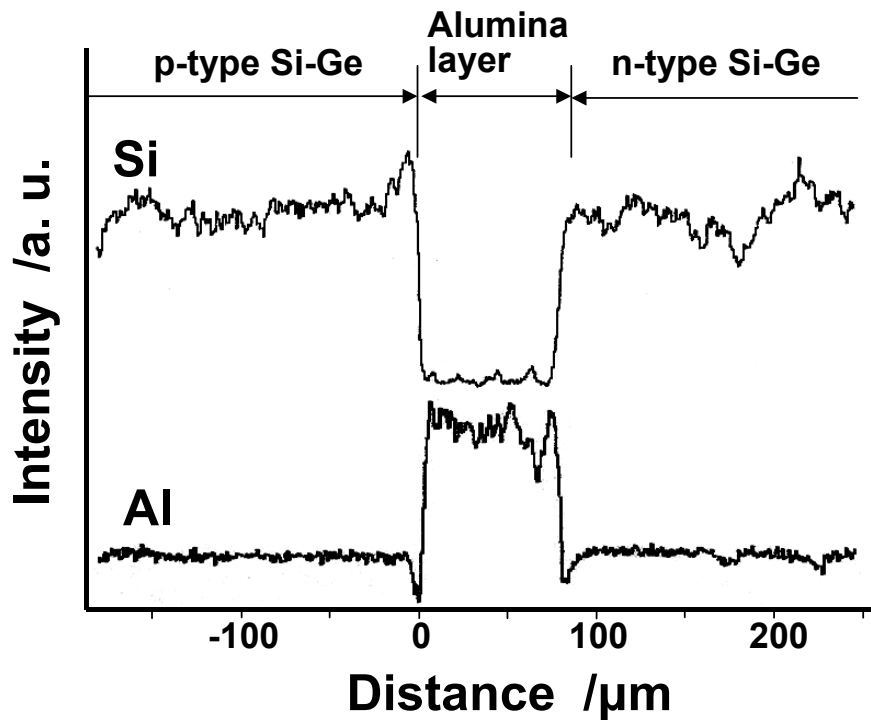


Fig. 4.8. Line profiles of Si and Al along p-n joint of joined element with an alumina layer.



Fig. 4.9. Joined Si-Ge element with a slit heated by a frame.

between Si-Ge and Al₂O₃ of 4.5×10^{-6} ²¹⁾ and 8.8×10^{-6} K⁻¹, ²²⁾ respectively. The adhesion between Si-Ge and alumina layer was probably improved by heating at a high temperature near the melting point of Si-Ge for sintering and joining, although some microporous seemed to exist inside the alumina layer. The line profiles of Si and Al shows that the intensity of Si in both types Si-Ge decreased abruptly at both interfaces and became almost constant inside the alumina layer, while that of Al was complementary, as illustrated in **Fig. 4.8**. That is, Al₂O₃ existed without a significant reaction within the Si-Ge even after sintering, which may be attributed to the very short time of the PCS process.⁷⁾ It was ascertained that these joined elements generated electric power when the p-n junctions were heated, as shown in **Fig. 4.9**.

4.3.2 Output of joined element

The output of a thermoelectric element increases with a temperature difference (ΔT) and decreases reversely with an increase in internal resistance,²³⁾ which is affected with the configuration shown in **Fig. 4.3**. Then, the effect of the configuration on the output of the joined element was studied. The voltage decreased linearly as the electric current increased, as shown in **Fig. 4.10**. The open voltage (V_0), which is the voltage at the current zero, varied with the temperature difference in the joined element.²⁾ The slope of the V - I straight line corresponded to the internal resistance (r) including the contact resistance between the element and conducting wire. The variations of the open voltage and the slope of the straight line were introduced from the effect of the configuration on the output of the joined element. The ΔT increased with l_i at constant l and with a decrease in l at constant l_i , as shown in **Table 4.2**. That is, the ΔT increased with l_i/l . The increase in l_i/l did not cause significantly r to increase except the No.4, led to the rise of the P_{max} . The relatively large l_i/l was efficient for the increase in the output. For the contrary ΔT and r parameters, the output of FeSi₂ joined element with the dimensions $l = 15.4$ mm, $w = 7.4$ mm and $t = 7.3$ mm increased with l_i/l and showed the maximum value at $l_i/l = 0.6$,¹³⁾ although that of the Si-Ge

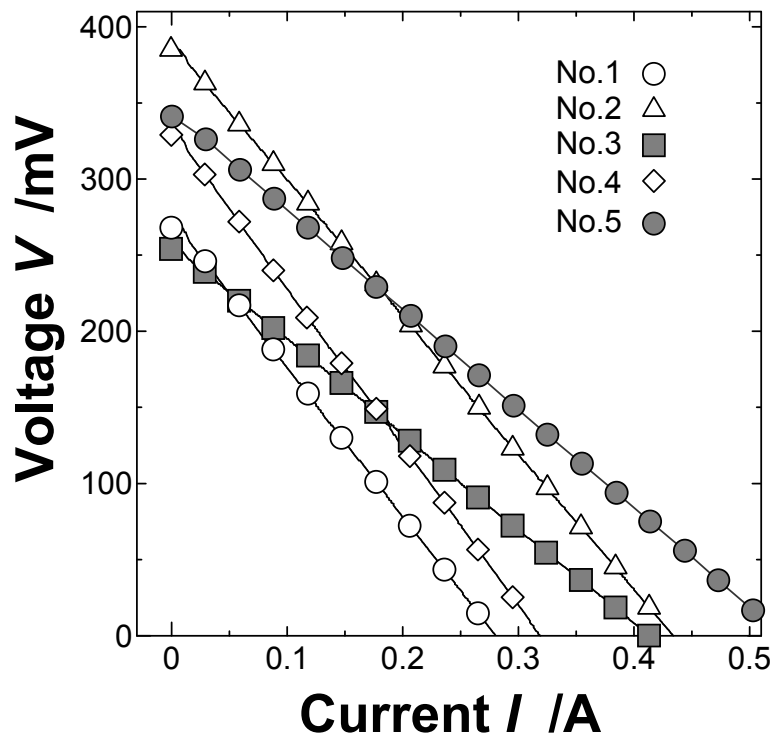


Fig. 4.10. Relationship between the output voltage V and electric current I of joined elements with a slit.

Table 4.2. Output of Joined Element with a Slit and an Alumina Layer

Sample	I_j / I	T_h' /K	T_c /K	ΔT /K	r / Ω	V_0 /V	P_{max} /mW
No.1	0.50	972	658	314	1.0	0.27	19
No.2	0.77	1136	648	488	0.9	0.38	42
No.3	0.63	1053	635	418	0.6	0.25	26
No.4	0.75	1130	657	473	1.1	0.33	27
No.5	0.90	1220	595	625	0.8	0.34	46
No.6*	0.90	1223	638	585	0.9	0.41	49

* Joined element with an alumina layer in the same configuration as No.5.

joined element in this study increased monotonically up to $l_i/l = 0.9$. The increase in l_i/l seems to cause the decrease in the strength of the p-n junction, thus the insertion of an alumina layer will be preferable.

The thermal conductance (K) is obtained from the following equation (4.2) :²³⁾

$$K = \kappa (A / L), \quad (4.2)$$

where κ is thermal conductivity, A cross sectional area and L length of the element, respectively. The decreased cross sectional area as the same as the increased l_i/l may contribute to an increase in its ΔT due to the small thermal conductance. As a result, No. 5 had the largest output of 46 mW among these elements, followed by No.2.

As shown in **Fig. 4.11**, the V - I straight lines of No.5 were obtained between 473 and 1273 K for the clarification of the temperature dependence on P_{max} , together with the the joined element No. 6 with an alumina layer, which was the same configuration as No.5. It was found that the joined elements with a slit and an alumina layer had almost the same output ability. The outputs of these elements were proportional to the second order of heating temperature. The slope of the output curve of the joined element with an alumina layer became slightly steeper than that of the joined element with a slit in the temperature range beyond 1000 K. The P_{max} of the joined element with an alumina layer was 49 mW when heated at 1273 K, as shown in **Table 4.2**, which was 3 mW larger than that of the slit-introduced one due to large open voltage. Furthermore, the output increased possibly up to 64 mW when the cold end of the joined element was cooled down to 552 K by air-blowing. This value is reduced to 28 Wkg⁻¹. This was slightly lower than the Noguchi's value (30 Wkg⁻¹) of the joined element with a slit.¹⁴⁾ This slight difference was probably due to the higher contact resistance of No.6 than the Noguchi's one. It was not clear that No.6 had large open voltage despite of small ΔT , of which the detailed expression must await further study.

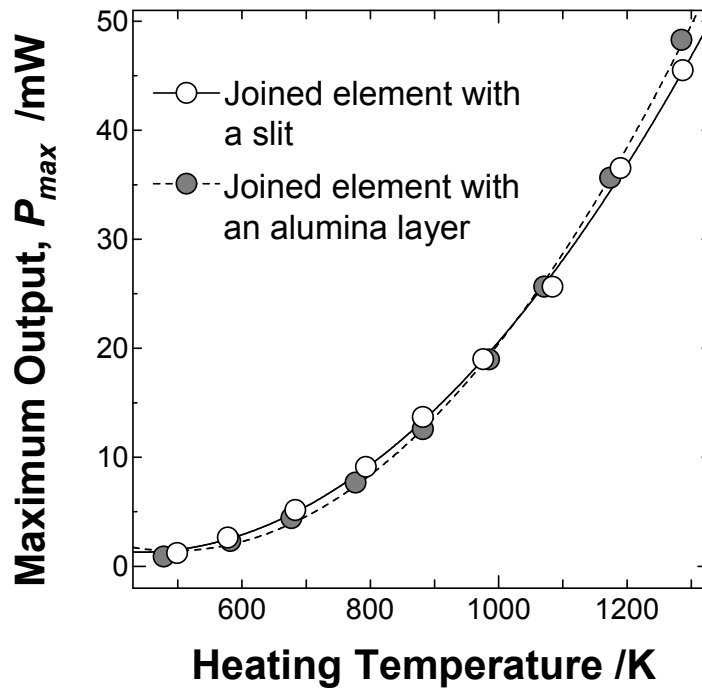


Fig. 4.11. Outputs of joined elements with a slit and an alumina layer as a function of heating temperatures.

4.4 Summary

Two types of p-n joined $\text{Si}_{0.8}\text{Ge}_{0.2}$ thermoelectric elements were fabricated by pulse-current sintering of the corresponding gas-atomized powders: A joined element was obtained by making a slit between the p- and n-type dense bodies after unified by the sintering; another element had an alumina layer sandwiched instead of a slit for strengthening. The p-n joints of both elements were firmly connected without any crack. The alumina layer inserted existed likewise as it had been even after sintered, which may be attributed to a very short sintering time. The outputs of these elements were strongly dependent on their configurations of length of element l , depth of slit l_i , and width of element leg w . The configuration of $l=26$ mm, $l_i=24$ mm, and $w=2.5$ mm gave the maximum outputs of 46 and 49 mW without and with an alumina layer at 1273 K, respectively. It was shown that the insertion of an alumina layer increased the output of the thermoelectric element.

References

- 1) Rowe, D. M., "CRC Handbook of Thermoelectrics," Ed. by Rowe, D. M., CRC Press, London, U. K. (1995) pp.1-5.
- 2) Wood, C., *Rep. Prog. Phys.*, Vol.**51**, pp.459-539 (1988).
- 3) Rowe, D. M., *J. Power Sources*, Vol.**19**, pp.247-259 (1987).
- 4) Vining, C. and Fleurial, J. P., "Silicon Germanium, An overview of recent developments," Ed. by Rowe, D. M., Babrow Press, Cardiff, United Kingdom (1991), pp.1-14.
- 5) Miller, S. A., Feingold, E. and Vining, C. B., *Modern Developments in Powder Metallurgy*, Vol.**17**, pp.671-682 (1985).
- 6) Otake, M., Sato, K., Sugiyama, O. and Kaneko, S., *J. Ceram. Soc. Jpn.*, Vol.**111**, pp.748-754 (2003).
- 7) Kim, H. T., Kawahara, M. and Tokita, M., *Powder Powder Metal.*, Vol.**47**, pp.887-891 (2000).
- 8) Otake, M., Sato, K., Sugiyama, O. and Kaneko, S., *J. Ceram. Soc. Jpn.* Vol.**111**, pp.907-911 (2003).
- 9) Kajikawa, T., "Thermoelectrics, Principals and Applications," ed. by Sakata, R., Realize, Tokyo (2001), pp.130-153. [in Japanese]
- 10) Nakajima, T., Suzuki, M. and Ohta, J., Proc. 16th Intersociety Energy Conversion Engineering Conf., pp.2013-2018 (1981).
- 11) Iwamoto, T. and Tokita, S., Proc. 17th Int. Conf. on Thermoelectrics, pp.456-459 (1998).
- 12) Stohrer, U., Voggesverger, R., Wagner, G. and Birkholz, U., Proc. 8th Int. Conf. on Thermoelectric Energy Conversion, pp.130-132 (1989).
- 13) Gross, E., Powalla, M. Stohrer, U. and Birkholz, U., Proc. 9th Int. Conf. On Thermoelectrics, pp.336-342 (1990).
- 14) Noguchi, T., Proc. 16th Int. Conf. on Thermoelectrics, pp.207-214 (1997).

- 15) Shin, W., Murayama, N., Ikeda, K. and Sago, S., *Jpn. J. Appl. Phys.*, Vol.**39**, pp.1254-1255 (2000).
- 16) Ikoma, K., Munekiyo, M., Furuya, K., Kobayashi, M., Izumi, T. and Shinohara, K., Proc. 17th Int. Conf. on Thermoelectrics, pp.464-467 (1998).
- 17) Matsubara, K., Proc. 2001 Japan Symp. Thermoelectric Conversion (TEC2001), pp.94-99 (2001). [in Japanese]
- 18) Matsuura, K., Rowe, D. M., Koumoto, K., Min, G. and Tsuyoshi, A., Proc. 11th Int. Conf. on Thermoelectrics, pp.10-16 (1992).
- 19) Cobble, M. H., Proc. 3rd Int. Conf. on Thermoelectric Energy Conversion, pp.78-81 (1980).
- 20) El-Genk, M. S., Seo, J. T. and Buksa, J. J., *J. Appl. Phys.*, Vol.**61**, pp.2059-2064 (1987).
- 21) Vining, C. B., "CRC Handbook of Thermoelectrics," ed. by Rowe, D. M., CRC Press, London, U. K. (1995) p. 329-337.
- 22) Kingery, W. D., Bowen, H. K. and Uhlmann, D. R., "Introduction to Ceramics 2nd Ed," John Wiley & Sons, Inc., New York (1976).
- 23) Goldsmid, H. J., "CRC Handbook of Thermoelectrics," ed. by Rowe, D. M., CRC Press, London, U. K. (1995) pp.19-25.

Chapter 5 XPS analysis of p-n junction

5.1 Introduction

For thermoelectric element, the simultaneous sintering and joining of both types of semiconducting powder materials has an advantage of being electrode-free in the hot end.¹⁾⁻³⁾ These techniques are also effective for process simplification and cost reduction. However, it is known that the direct joining of p- and n-type semiconducting materials frequently brings about the reduction of electric power generation caused by the occurrence of a high-resistivity interlayer due to the interdiffusion of both dopants during sintering.^{4),5)}

The penetration depth of dopants may be determined based on X-ray photoelectron spectroscopy (XPS) profiles obtained in the vicinity of the p-n junction,⁶⁾ because the profiles provide information on the distinction between p- and n-type semiconductors by measuring the binding energies of major constituent elements without the direct determination of dopants. For obtaining good thermoelectric materials, the state between p- and n-type semiconductors must be clarified. In this chapter, p-n joined Si-Ge sintered bodies were fabricated by sintering and joining using this technique, and the penetration behavior of both boron and phosphorous as dopants in the vicinity of the p-n junction of this sample was elucidated by XPS.

5.2 Experimental

5.2.1 Sample preparation

A p-n joined Si-Ge sintered body (hereafter abbreviated as p-n joined Si-Ge) 20 mm in diameter and 7.5 mm in thickness was fabricated by the procedure shown in **Fig. 5.1** using p- and n-type Si-Ge powders prepared separately with a gas atomizing system.⁷⁾ Chemical compositions of p- and n-type powders obtained were Si 79.7 mol%, Ge 20.1 mol%, B 0.21 mol%, and Si 79.8 mol%, Ge 20.0 mol%, P 0.18 mol%, respectively. Then p- and n-type powders of 3 g each were charged in turn in a cylindrical carbon vessel 20 mm in diameter,

and subjected to sintering for 180 s at 49 MPa with a PCS apparatus.⁸⁾ The carbon vessel was enclosed with a carbon thermal insulator to realize the temperature uniformity of the powders. The sintering temperature of 1503 to 1523 K was measured with a Pt-(Pt-13 %Rh) thermocouple, the head of which was inserted into the vessel wall adjacent to the sintering sample.

5.2.2 XPS analysis

The p-n joined Si-Ge were ground at 0, 1.7, 2.4, 3.2, 3.3, 3.5, 3.8, 4.1, 4.6, 5.2, 5.7, and 7.4 mm each from the p-type surface with Al₂O₃ abrasive paper. Photoelectron spectra of Si2s and Ge3d were obtained using a spectrophotometer (Model XSAM 800 pci. Shimadzu-Kratos, Kyoto, Japan) using AlK α radiation with an output of 15 kV and 10 mA. The absolute value

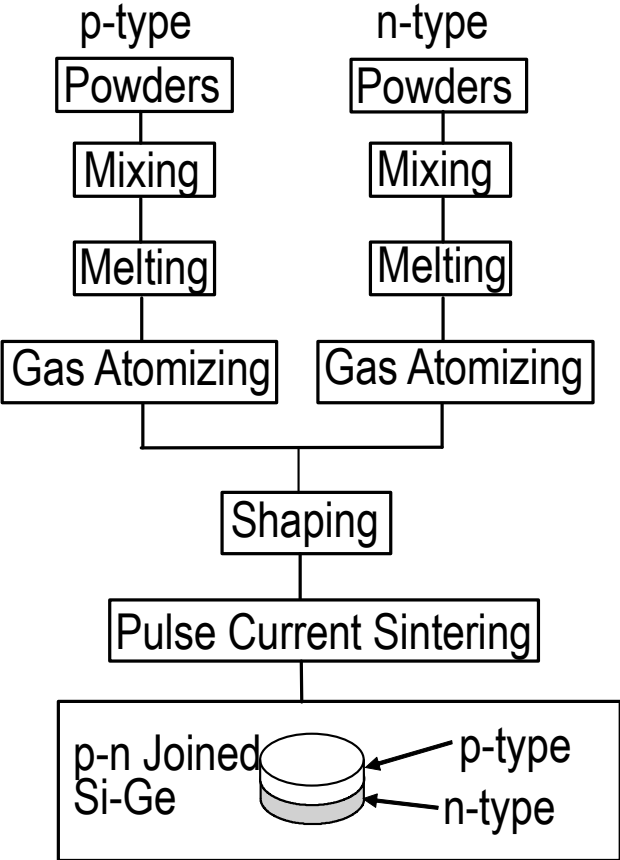


Fig. 5.1. Sample preparation procedure.

Table 5.1. Conditions of XPS Analysis

Peak	Scan range		Scan step	Sampling time	Number of scans
	/eV		/eV	/ms	
Si2s	143~	163	0.05	298	5
Ge3d	24~	34	0.05	594	5
C1s	280~	310	0.05	99	5

of the binding energy was calibrated with the C1s energy of 285.0 eV that was obtained from hydrocarbon molecules absorbed on the sample. The photoelectron spectra obtained were processed with the VISION Version 1.4.0 data processing system (Kratos Analytical Ltd., England). The analytical conditions employed are summarized in **Table 5.1**.

5.3 Results and discussion

5.3.1 Binding energy

The spectra in **Fig. 5.2** show differences in the binding energy of both Si2s and Ge3d between p- and n-type Si-Ge samples. The observed peak binding energies of p- and n-type samples of Si2s were 149.8 and 150.3 eV, and those of Ge3d were 28.5 and 29.1 eV. The distinction between the p- and n-type layers of the joined p-n Si-Ge is also available by XPS. The energy differences of Si2s and Ge3d between p- and n-type samples are 0.5 and 0.6 eV, respectively. The difference in the binding energy of Si2p between the p- and n-type silicon semiconductors has already been reported,⁹⁾ but here, the difference in the binding energy of Ge3d between the p- and n-type Si-Ge semiconductors is first observed.

Figure 5.3 shows Si2s and Ge3d photoelectron spectra measured at various distances from the p-n junction of the p-n joined Si-Ge. The binding energy determined from the top of each spectrum is summarized in **Table 5.2**, where the binding energies at 3.5 mm from the p-n junction ① and 3.9 mm in the opposite direction ⑥ were the same as those of p-type and n-type Si-Ge samples, respectively. Both the binding energies of Si2s and Ge3d

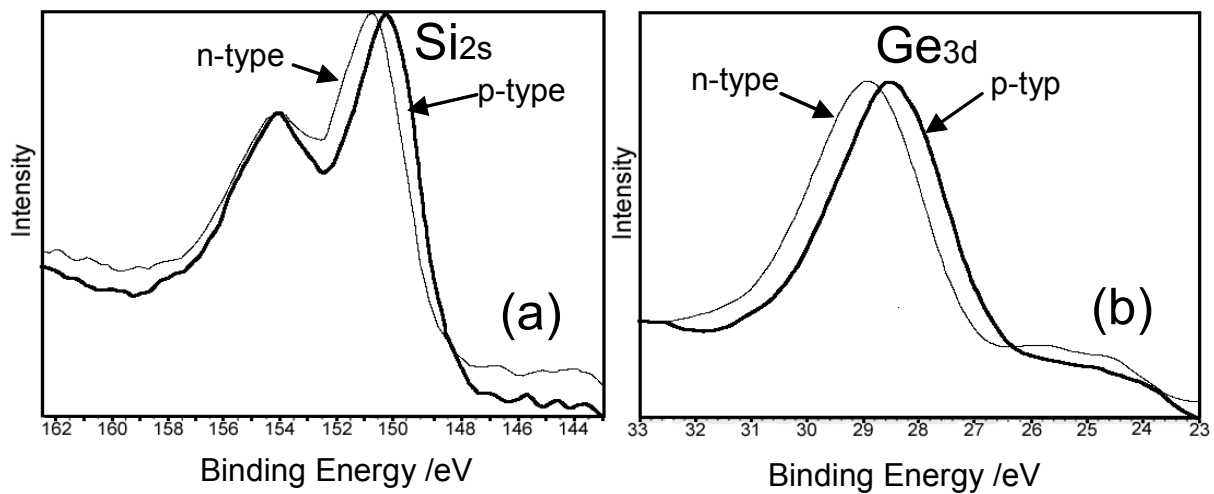


Fig. 5.2. (a) Si_{2s} and (b) Ge_{3d} photoelectron spectra of p- and n-type SiGe samples

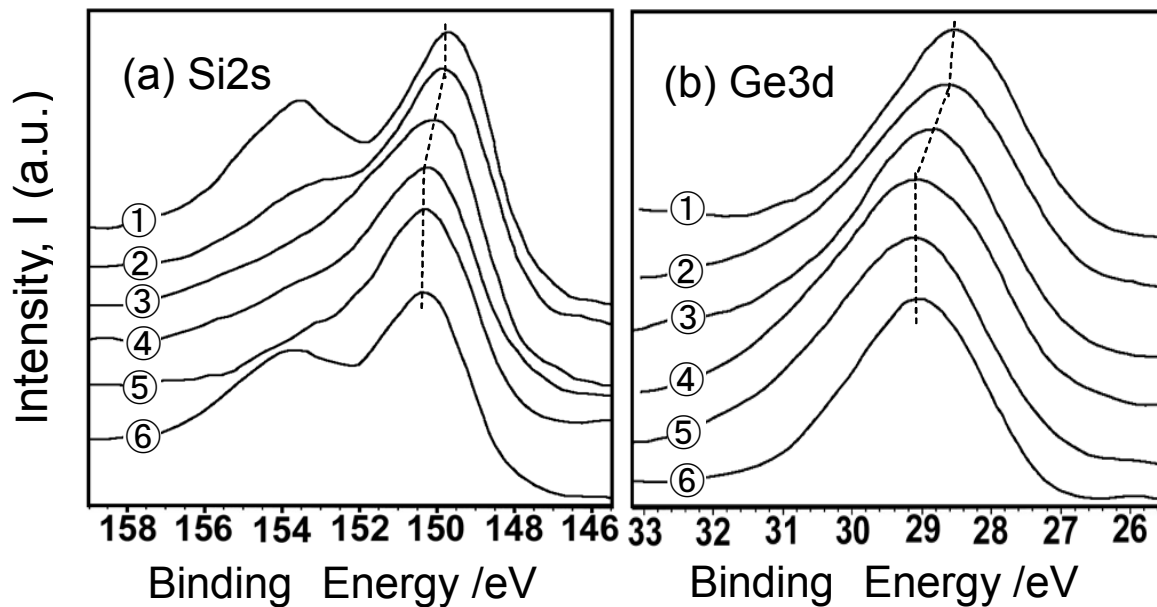


Fig. 5.3. Change in (a) Si_{2s} and (b) Ge_{3d} photoelectron spectra of the p-n joined Si-Ge along the thickness direction. The notations ① to ⑥ correspond to the numbers ① to ⑥ in Table 5.2, respectively.

Table 5.2. Binding Energies of p-n Joined Si-Ge

	Position No.	Distance from p-n junction /mm	Si2s Binding energy /eV	Ge3d Binding energy /eV
p-type layer	①	-3.5	149.8	28.5
	②	-1.1	149.9	28.7
	③	-0.35	150.1	28.9
n-type layer	④	0.3	150.3	29.1
	⑤	1.1	150.4	29.1
	⑥	3.9	150.3	29.1

at position ② in the p-type side are almost the same as those at position ①, however, those at position ③ become somewhat larger and are close to the values of the n-type side. The binding energies of Si2s and Ge3d at positions ④ and ⑤ in the n-type side are the same as those at position ⑥. The increase in the binding energies at position ③ presumably implies the formation of the interlayer only in the p-type side. Furthermore, another peak of Si2s at positions ① and ⑥ is observed at around 154 eV, which corresponds to SiO_x.

5.3.2 Formation of interlayer

The relationship between the binding energies of Si2s and Ge3d of joined Si-Ge and the distance from the p-n junction are shown in **Figs. 5.4(a)** and **(b)**, respectively. Both the binding energies of Si2s and Ge3d increase gradually from the original value of the p-type Si-Ge when measured closer to the p-n junction. On the other hand, in the n-type side the energies of Si2s and Ge3d are almost constant. As a result, the interlayer of about 2mm seems to be formed as illustrated schematically in **Fig. 5.5**. Increasing the sintering temperature could promote the diffusion of boron and phosphorus toward the opposite side

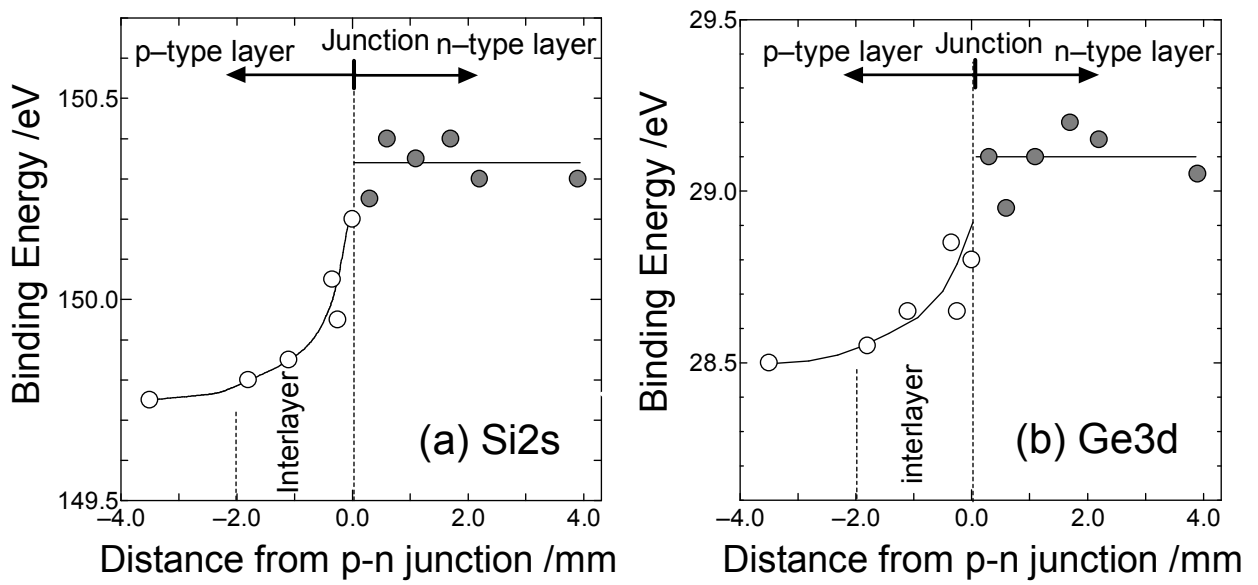


Fig. 5.4. Relationships of the binding energies and the distance from a p-n junction. (a) Si2s photoelectron and (b) Ge3d photoelectron.

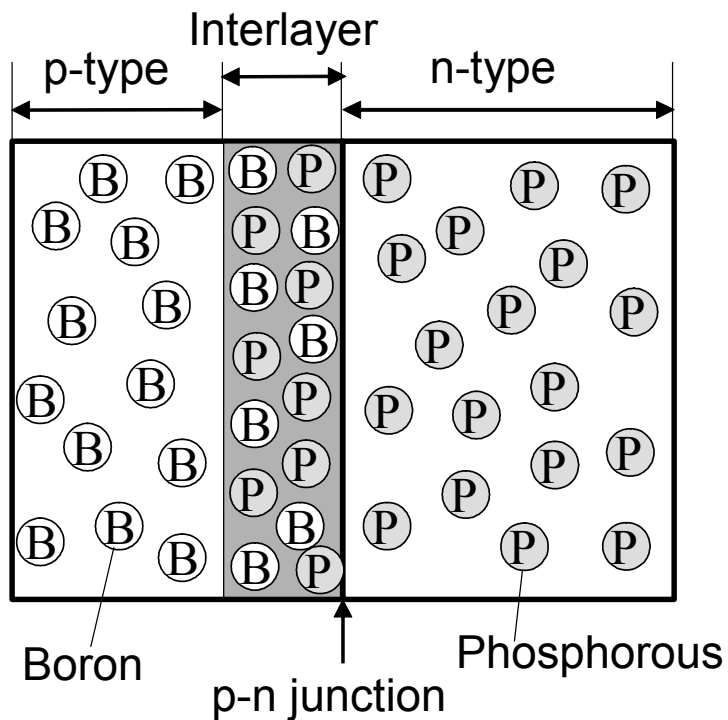


Fig. 5.5. Schematic illustration of the diffusion of dopants in the vicinity of a p-n junction after sintering and joining.

through the junction. The diffusion coefficients D of boron and phosphorous in silicon at a sintering temperature, 1523 K, are reported to be 9.88×10^{-16} and $6.5 \times 10^{-16} \text{ m}^2\text{s}^{-1}$, respectively.¹⁰⁾ When boron and phosphorus diffuse in silicon at 1523 K for 1200 s, the diffusion distances ($=2(Dt)^{0.5}$, t : time) of boron and phosphorus are estimated to be 0.0022 mm and 0.0018 mm. Taking into consideration the observed diffusion distance of phosphorous which is much longer than the calculated value and the low boiling point at 998 K, the migration of phosphorus may occur by the vaporization-condensation mechanism across the p-n junction. The migration of boron was not recognized at all. Thus, the interlayer was only formed in the p-type side. Noguchi et al. found the interlayer with a high electrical resistivity of approximately $500 \text{ m}\Omega \cdot \text{cm}$ in the vicinity of the p-n junction of joined Si-Ge.⁴⁾

XPS analysis was proved to be one of the most effective methods for the characterization of the p-n junction, and performance is expected to improve by using this XPS technique.

5.4 Summary

The penetration behavior of dopants, boron and phosphorous, across a p-n junction in a joined silicon-germanium semiconductor, which had been applied to a thermoelectric element, was elucidated by X-ray photoelectron spectroscopic (XPS) analysis. The p-n joined disk sample was prepared from Si, Ge and B (79.7: 20.1: 0.21 in atomic ratio for p-type semiconductor), and Si, Ge and P (79.8: 20.0: 0.18 for n-type) powders one on the top of the other at 1523 K for 180 s under 49 MPa by a pulse current sintering process. Then, the XPS measurement and surface grinding of the joined sample were carried out alternately, which gave a series of photoelectron spectra as a function of distance from the p-n junction. The binding energy differences for Si2s and Ge3d peaks between the p-type and the n-type sides were 0.5 and 0.6 eV, respectively. An interlayer with a thickness of approximately 2 mm was found just in the p-type side judging from the above energy differences. The binding energies inside the interlayer along the thickness varied gradually between the

original value of p-type Si-Ge and that of the n-type. It was considered that both the dopants coexisted in the interlayer, caused by the migration of phosphorous of the n-type side into the p-type side. The long-distance migration of phosphorous more likely occurred according to the vaporization-condensation mechanism. XPS analysis was proved to be most effective for the characterization of the p-n junction of semiconductors.

References

- 1) Iwamoto, T. and Tokita, S., Proc. 17th Int. Conf. on Thermoelectrics, pp.456-459 (1998).
- 2) Noguchi, T., Proc. 16th Int. Conf. on Thermoelectrics, pp.207-214 (1997).
- 3) Shin, W., Murayama, N., Ikeda, K. and Sago, S., *Jpn. J. Appl. Phys.*, Vol.39, pp.1254-1255 (2000).
- 4) Noguchi, T., Masuda, T. and Nitta, J., Proc. 17th Int. Conf. on Thermoelectrics, pp.406-409 (1998).
- 5) Yang, J. Y., Abstr. Spring Meeting Japan Soc. Powd. and Powd. Metall., p.198 (2000).
- 6) Briggs, D. and Seah, M. P., "Practical Surface Analysis - 2nd Ed. Vol.1 Auger and X-ray Photoelectron Spectroscopy," John Wiley & Sons Ltd., U. K. (1990).
- 7) Lowley, A., *J. Metals*, pp.1-13 (1981).
- 8) Omori, M., *Mater. Sci. Eng.*, A287, pp.183-188 (2000).
- 9) Moulder, J. F., Stickle, W. F., Sobol, P. E., Bomben, K. D., "Handbook of X-ray Photoelectron Spectroscopy," Ed. by Chastain J., Perkin-Elmer Corporation (1992) p.238.
- 10) National Astronomical Observatory "Chronological Scientific Tables," Maruzen Co. (1997) p.470. [in Japanese]

Chapter 6 Multilayered Si-Ge Thermoelectric Element and Module

6.1 Introduction

For the reduction of energy consumption and the sustainable global environment, research work on thermal-electrical energy conversion has increased resulting in the development of effective thermoelectric materials.¹⁾²⁾ Thermoelectric element is usually fabricated by bridging each end of p- and n-type semiconductors with a metal plate, which yields electrical power by making use of a temperature difference between both ends of this bridged element.³⁾⁴⁾ Silicon-germanium (Si-Ge) is one of thermoelectric materials used in a temperature range of 500-1000°C.⁵⁾ In previous chapter, we studied the thermoelectric properties of p- and n-type Si-Ge dense bodies fabricated by pulse-current sintering (PCS) of the corresponding gas-atomized powders,⁶⁾ where both figures of merit, ZT , increased monotonically with temperature until 1073 K, and became 0.56 and 0.66, respectively.

Also, thermoelectric element was possibly obtained by joining both types of semiconductors directly without metal plate, where a slit was inserted between them except a high temperature part.⁷⁾ Thermoelectric elements using Si-Ge,⁸⁾ $\text{Li}_{0.025}\text{Ni}_{0.975}\text{O}-\text{Bi}_{0.4}\text{Sr}_{0.6}\text{PbO}_3$,⁹⁾ and $\beta\text{-FeSi}_2$ ¹⁰⁾ used at high temperatures were fabricated by this process. A p-n joined $\text{Si}_{0.8}\text{Ge}_{0.2}$ thermoelectric element with a sandwiched alumina layer for strengthening (hereafter, abbreviated as joined element) was attempted to fabricate by simultaneous sintering and joining of the corresponding Si-Ge gas-atomized powders and an alumina cloth, however, the output of this joined element was proved to be insufficient.¹¹⁾ Thus, many elements should be connected electrically to increase the output for practical applications. In this chapter, a multilayered element was made by direct and repeated stacking with p- and n-type semiconductors, as illustrated in **Fig. 6.1(a)**. On the other hand, the fabrication of a module was attempted by the connection of sixteen pairs of the joined elements with conductive wires, as shown in **Fig. 6.1(b)**.

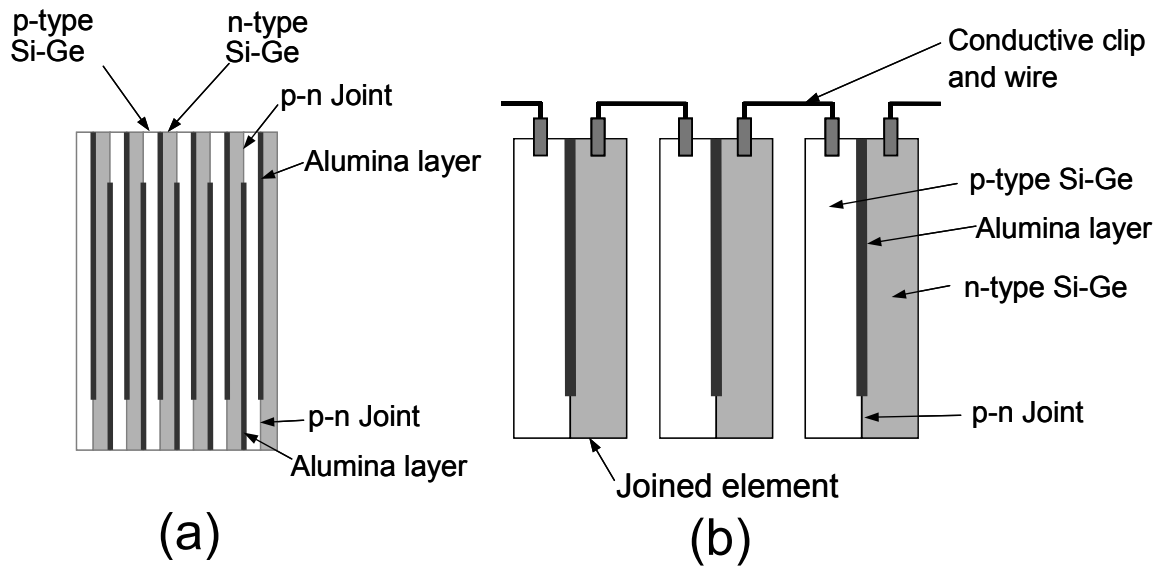


Fig.6.1. Multilayered element (a) and thermoelectric module (b).

6.2 Experimental

6.2.1 Fabrication of multilayered element and module

Both p- and n-type Si-Ge powders were prepared by gas atomization technique, as described in a previous chapter.¹²⁾ Chemical compositions of p- and n-type powders obtained were Si 79.7 mol%, Ge 20.1 mol%, B 0.20 mol%, and Si 79.8 mol%, Ge 20.0 mol%, P 0.20 mol%, respectively.

Multilayered element was fabricated by following procedures: Alumina cloth of 30 mm in diameter and 2mm in thickness (NICHIAS No.5475, Japan) as an insulator was sandwiched with p- and n-type Si-Ge powders of 1g each, which were charged ten times in a cylindrical carbon vessel with an inner diameter of 30 mm. Then it was uniaxially compressed with a carbon punch at 49 MPa. The alumina cloth was cut off partly for the direct contact between the p- and n-type Si-Ge powders in advance. The simultaneous sintering and joining were carried out by heating at 1523 K for a soaking time of 180 s in vacuo using a PCS apparatus (Sumitomo Coal Mining SPS-1030). As-sintered body of 30 mm in diameter and 15 mm in thickness was further processed into rectangle shape by a cutting machine (**Fig. 6.1(a)**). Nickel plates were welded on p- and n-type surfaces of both

ends of the multilayered element with silver solder prior to the output measurement.

Si-Ge thermoelectric module was fabricated using sixteen pairs of the joined elements. Each joined element composed of the module was 26 mm × 5.0 mm × 5.5 mm in size and 1.0 Ω in resistance. Each cold end was plated with nickel for the reduction of the contact resistance. The elements arranged in 4 × 4 of the module were surrounded by alumina clothes in a hollowed brick as a container for the isolation and insulation. And then all the p- and n-type cold ends were connected in series with conductive clips and wires (**Fig. 6.1(b)**).

6.2.2 Measurement of output

The output of a sample was determined by using a measurement system composed of heating controller and electrical measurement devices, as described in chapter 5.¹¹⁾ The hot end of a sample was inserted to the furnace through the upper board, where it was heated at the prescribed temperatures ranging from approximately 473 to 1273 K. Voltage and electric current generated from a sample were measured with data logger at each temperature. After a starting signal was sent from a trigger generator, voltage (V), electric current (I), and temperatures at both hot and cold ends (T_h and T_c) were monitored by the data logger while the electric current through a sample was controlled from 0 to 1.0 A by an electronic load device in 5 s. The maximum output (P_{max}), which was the maximum value of the multiplication of electric current and voltage, was calculated for the evaluation of a sample.

6.3 Results and discussion

6.3.1 Multilayered element

Figure 6.2 shows the appearance of multilayered element with 20 layers of p- and n-type Si-Ge semiconductors with approximately 15 mm × 25 mm × 14 mm in size and 14.7 g in weight. The p-n joints of the multilayered element obtained with 15 mm × 25 mm × 14 mm in size were firmly connected without any crack. The alumina layers become thinner and blackish via the PCS process. The widths of Si-Ge and alumina layers were

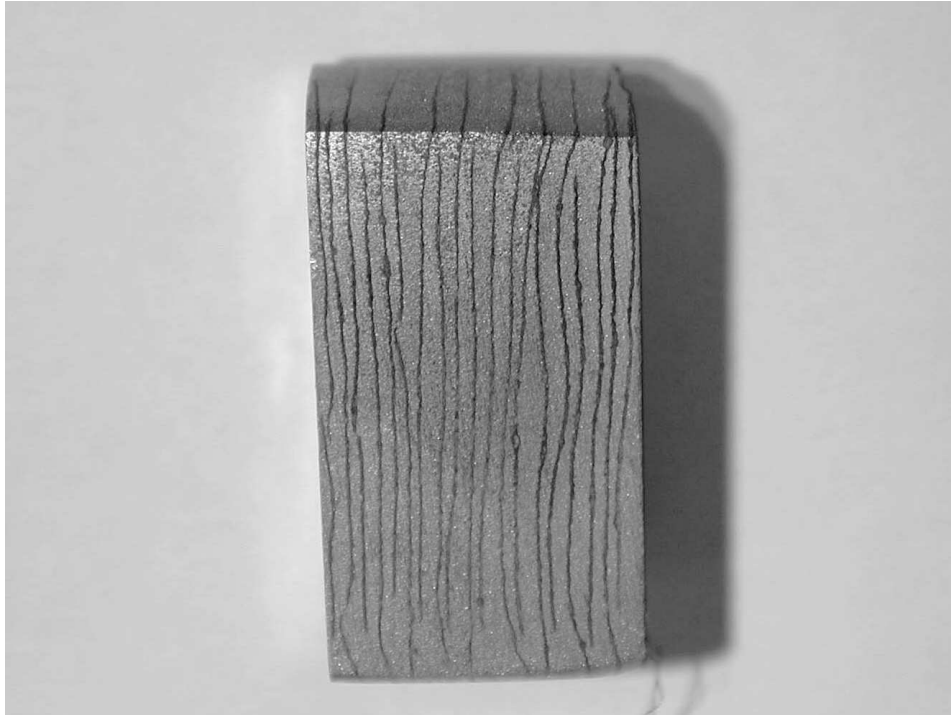


Fig. 6.2. Multilayered element with alumina layers.

approximately 600 and 80 μm , respectively. The alumina layers existed without a significant reaction within the Si-Ge even after the sintering process, which may be attributed to the short sintering time of the PCS process.

Figure 6.3 shows that high open voltage was obtained at a high heating temperature due to a large temperature difference, as likely as short circuit current. The slopes of these straight lines mean the internal resistance including the contact resistance between the element and the conductor. The slopes of these lines gradually decreased as the heating temperature increased. The internal resistance of this element was 1.95 Ω on average in the heating temperature range of 478-1277 K.

The maximum output P_{max} of the element was determined at each heating temperature, compared with that of joined element, as shown in **Fig. 6.4**. Here, both the P_{max} of these elements were proportional to the second order of the temperature difference, as expected from the theoretical consideration.¹³⁾ The difference in P_{max} between these elements

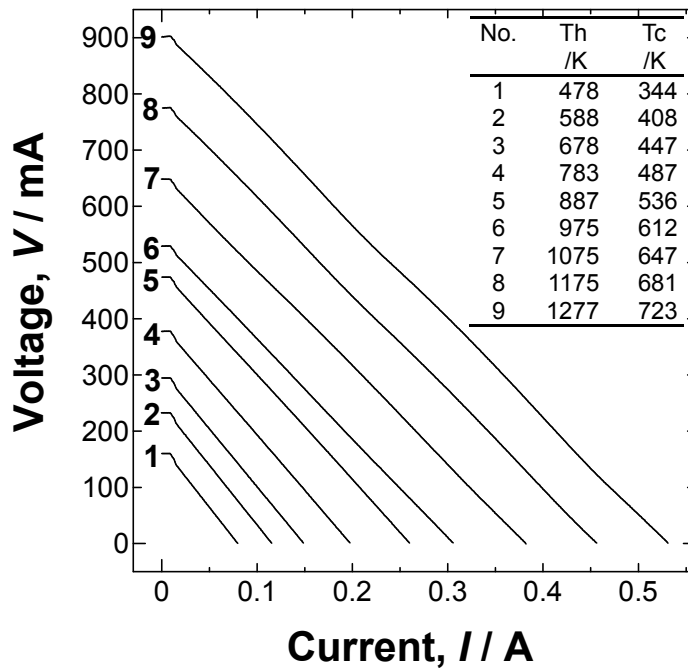


Fig. 6.3. Relation between output voltage and electric current of multilayered element with various heating temperatures.

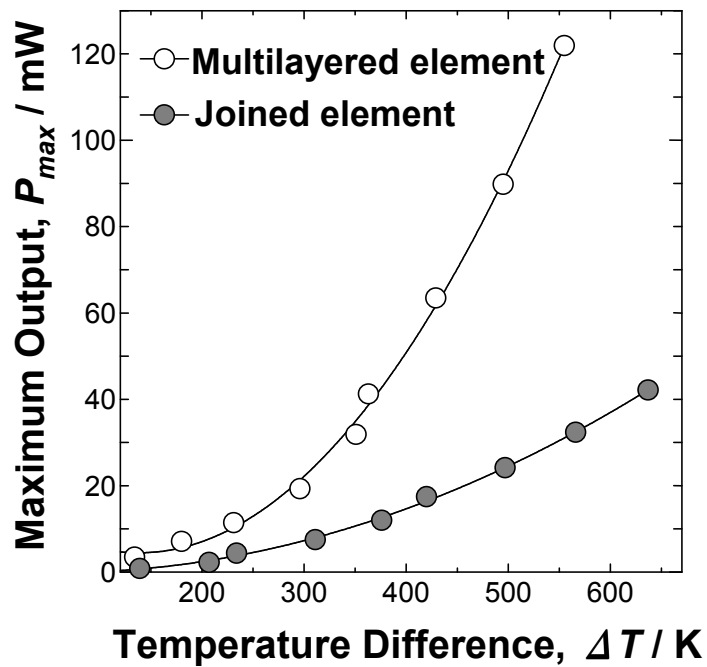


Fig. 6.4. Maximum outputs P_{max} of multilayered and joined elements.

increased as the temperature difference increased, giving the effectiveness of the multilayered element. The P_{max} of the multilayered element was approximately 3.5 times larger than that of joined element when the temperature difference is 500 K.

6.3.2 Comparison with module

The appearance of the module with 78 mm × 95 mm × 65 mm in size and its output were shown in **Fig. 6.5** and **Table 6.1**, respectively. The P_{max} of the module was 1.4 W when heated at 1273 K. This value increased up to 2.0 W when the cold side of the module was further cooled down to 289 K by air-blowing. The conductive clips for connecting the elements electrically also promote to cool down the cold side of the module. This module was experimentally applied for the power generator for the charge of nickel metal hydride (NiMH) batteries, as shown in **Fig. 6.6**.

The internal resistance r , temperature differences ΔT and the output at 1273 K of the joined and multilayered elements and module are summarized in **Table 6.1**. The output per one pair of the module was the highest, while that of the multilayered element was the lowest almost in accordance with the ΔT . The large ΔT of the module was attributed to the large cooling effect of the conductive clips. On the other hand, the small ΔT of the multilayered element was due to its large cross sectional area caused by multilayering, which agrees with the result about the configurative dependence of the joined element on its output.¹¹⁾ As a result, multilayering was found to have the disadvantage of small temperature difference, but it may be improved by the use of cooling water or fin. It is expected that the multilayering technique will be applied to the fabrication of the thermoelectric power generator because the technique have many advantages such as a supply of higher voltage, a requirement of few numbers of thermoelectric assemblies and resultant weight saving of the module.

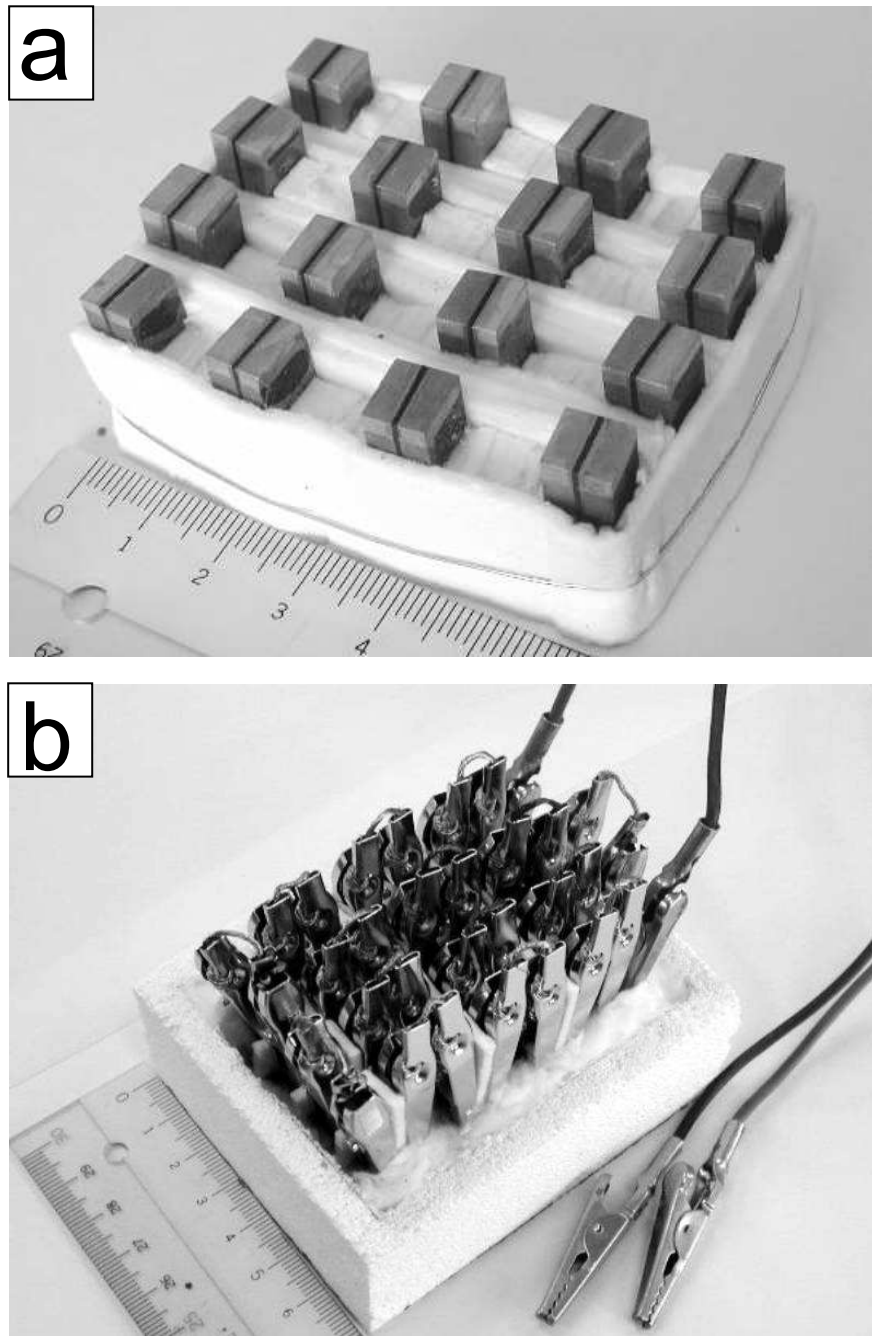


Fig. 6.5. Appearance of Si-Ge thermoelectric module by using 16 elements.
Before (a) and after (b) the connection of the elements.

Table 6.1. Comparison of Element and Module.
 ($T_h = 1273 \text{ K}$)

	Internal Resistance	Temperature Difference	Output	
	r / Ω	$\Delta T / \text{K}$	Total P / mW	One pair P / mW
Joined element	0.9	647	48	48
Multilayered element	1.7	495	120	12
Module without air blowing	3.3	778	1400	88
Module with air blowing	3.3	864	2000	125

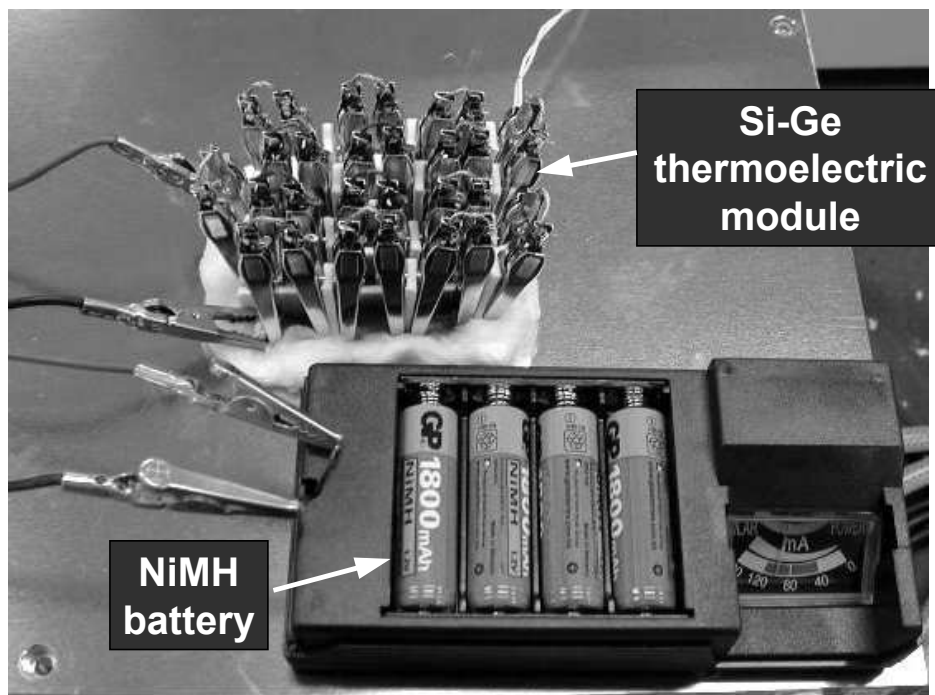


Fig. 6.6. The charge of batteries by Si-Ge thermoelectric module.

6.4 Summary

An alumina-inserted Si-Ge thermoelectric element with 20 Si-Ge layers was fabricated by pulse-current sintering of p- and n-type gas-atomized powders. The maximum output P_{max} of the element was 120 mW when the temperature difference between hot and cold ends of the element is 500 K, which was approximately 3.5 times larger than that of joined element. Furthermore, Si-Ge thermoelectric module was also obtained by connecting 16 of joined elements in series. The P_{max} of the module was 2.0 W when the hot end of the element was heated at 1273 K and the cold end cooled down to 562 K by air blowing. It is effective for the output improvement to multilayer the element, though the output per one pair of the multilayered element was relatively low due to its low cooling effect.

References

- 1) Rowe, D. M., "CRC Handbook of Thermoelectrics," Ed. by Rowe, D. M., CRC Press, London, U. K. (1995) pp.1-5.
- 2) Rowe, D. M., *J. Power Sources*, Vol.**19**, pp.247-259 (1987).
- 3) Wood, C., *Rep. Prog. Phys.*, Vol.**51**, pp.459-539 (1988).
- 4) Kibayashi, Y., "Thermoelectrics, Principals and Applications," ed. by Sakata, R., Realize, Tokyo (2001) pp.329-348. [in Japanese]
- 5) Vining, C. and Fleurial, J. P., "Silicon Germanium, An overview of recent developments," ed. by Rowe, D. M., Babrow Press, Cardiff, United Kingdom (1991), pp.1-14.
- 6) Otake, M., Sato, K., Sugiyama, O. and Kaneko, S., *J. Ceram. Soc. Jpn.* Vol.**111**, pp.907-911 (2003).
- 7) Stohrer, U., Voggesverger, R., Wagner, G. and Birkholz, U., Proc. 8th Int. Conf. on Thermoelectric Energy Conversion, pp.130-132 (1989).
- 8) Noguchi, T., Proc. 16th Int. Conf. on Thermoelectrics, pp.207-214 (1997).
- 9) Shin, W., Murayama, N., Ikeda, K. and Sago, S., *Jpn. J. Appl. Phys.*, Vol.**39**,

pp.1254-1255 (2000).

10) Gross, E., Powalla, M., Stohrer, U. and Birkholz, U., Proc. 9th Int. Conf. On Thermoelectrics, pp.336-342 (1990).

11) Otake, M., Sato, K., Sugiyama, O. and Kaneko, S. (submitted to Journal of Electrochemical Society)

12) Otake, M., Sato, K., Sugiyama, O. and Kaneko, S., *J. Ceram. Soc. Jpn.*, Vol.111, pp.748-754 (2003).

13) Goldsmid, H. G., "CRC Handbook of Thermoelectrics," Ed. by Rowe, D. M., CRC Press, London, U. K. (1995) pp.19-25.

Chapter 7 Conclusions

For the reduction of energy consumption and the sustainable global environment, research work on thermal-electrical energy conversion has increased resulting in the development of effective thermoelectric materials. Silicon-germanium (Si-Ge) is one of the high-temperature thermoelectric materials used in a temperature range of 500-1000°C, which is fabricated by sintering of p- or n-type semiconducting powders. In this study, the combination of gas-atomizing and pulse-current sintering techniques was used to obtain Si-Ge sintered bodies, and the physical and thermoelectric properties of the starting powders and sintered bodies were elucidated. Furthermore, Si-Ge thermoelectric element and its module were fabricated, followed by the evaluation of their outputs.

In chapter 2, the characteristics and sinterability of gas-atomized Si-Ge powders were studied. Particular emphasis was placed upon the understanding of the effect of ball-milling. Both types of $\text{Si}_{0.8}\text{Ge}_{0.2}$ powders were prepared with boron or phosphorous by a gas-atomizing method, and then the dense bodies were formed from these two types of Si-Ge powders by pulse-current sintering. The densification of as-prepared powders was abruptly promoted above 1500 K, while, that sinterability of as-prepared powders was improved by ball-milling with the reduced crystallite size and the increased surface distortion. The pulse-current sintering of the gas-atomized powder and its ball-milled one could yield the shaped bodies with a density of more than 99 % at 1523 and 1433 K, respectively, only in 3min as a soaking time.

In chapter 3, the thermoelectricity of the Si-Ge dense bodies were determined at from room temperature to 1073 K. The effect of ball-milling on the thermoelectricity was also discussed. The ball-milling was expected to decrease the thermal conductivity then to improve the thermoelectricity. As expected, the thermal conductivities of p- and n-type Si-Ge dense bodies were decreased by 8 and 10%, respectively, by the ball-milling. However, this phenomenon was accompanied with an increase in electrical resistivity due to

the reduced grain size and increased oxygen content, resulting in the decrease in thermoelectricity by 13 and 8% for p- and n-type Si-Ge dense bodies, respectively. The application of the gas-atomized powder for fabricating Si-Ge sintered body has the advantage of the reduction in oxygen content and in electrical resistivity compared to the case of the pulverized powders.

In chapter 4 and 5, p-n joined Si-Ge element and module were fabricated and evaluated. Both p-n directly joined $\text{Si}_{0.8}\text{Ge}_{0.2}$ thermoelectric elements with a slit and an alumina layer between p- and n-type semiconductors was fabricated by simultaneous sintering and joining of both types of Si-Ge gas-atomized powders and alumina cloth. The outputs of these elements depended on their configuration. The configurations of the thermoelectric elements, the length of the element, ($l=26$ mm), the length of the slit ($l_f=23.5$ mm), and the width of the element legs ($w=2.5$ mm) led to the maximum output. It was found that the joined elements with a slit and an alumina layer showed almost the same output ability. The joined element with an alumina layer showed 64 mW as the maximum output when the hot end of the element was heated at 1273 K and the cold end was cooled down by air-blowing. Furthermore, the penetration behavior of dopants, boron and phosphorous across a p-n junction in a joined Si-Ge semiconductor was elucidated by x-ray photoelectron spectroscopic analysis. An interlayer with a thickness of approximately 2 nm was found in the p-type side.

In chapter 6, multilayered Si-Ge element and Si-Ge thermoelectric module were fabricated for obtaining higher output. These element and module had the maximum output of 122 mW and 2.0 W, respectively.

In conclusion, gas-atomizing and pulse-current sintering techniques were proved to be effective to fabricate Si-Ge dense body and p-n joined element in speedy and simple process compared to the conventional way.

Papers

- (1) Otake, M., Sato, K., Sugiyama, O. and Kaneko, S., "XPS Analysis of Dopant Penetration in Joined p-n Silicon-Germanium Semiconductor," *J. Ceram. Soc. Jpn.*, Vol. **111**, pp.436-438 (2003).
- (2) Otake, M., Sato, K., Sugiyama, O. and Kaneko, S., "Effect of Ball-Milling on Sinterability of Si-Ge Powders Prepared by Gas-Atomization of the Corresponding Melts," *J. Ceram. Soc. Jpn.*, Vol. **111**, pp.748-754 (2003).
- (3) Otake, M., Sato, K., Sugiyama, O. and Kaneko, S., "Thermoelectric Properties of p- and n-type Si-Ge Dense Bodies Obtained from Gas-Atomized and their Pulverized Powders by Pulse-Current Sintering," *J. Ceram. Soc. Jpn.*, Vol. **111**, pp.907-911 (2003).
- (4) Otake, M., Sato, K., Sugiyama, O. and Kaneko, S., "Sinterability and Thermoelectric Properties of p- and n-Type Si-Ge Powders Prepared by Gas-Atomizing Method," *J. Ceram. Soc. Jpn.* (Supplement Edition). (in Press)
- (5) Otake, M., Sato, K., Sugiyama, O. and Kaneko, S., "Pulse-Current Sintering and Thermoelectric Properties of Gas-Atomized Silicon-Germanium Powders," *Solid State Ionics*. (in Press)
- (6) Otake, M., Sato, K., Sugiyama, O. and Kaneko, S., "Fabrication and Output Evaluation of p-n Joined Si-Ge Thermoelectric Elements". (Submitted)
- (7) Otake, M., Sato, K., Sugiyama, O. and Kaneko, S., "Output Enhancement of p- and n-type joined Si-Ge Element by Integration and Connection". (Submitted)

Oral Presentations

- (1) Otake, M., Isobe, K. and Kosugi, T., "Fabrication of p-n Joined Silicon-Germanium Thermoelectric Element by Pulse-Current Sintering," p.428, Abstr. the 126th Spring Meeting on Japan Inst. Metals, Tokyo (2000).
- (2) Otake, M., Isobe, K., Sato, K., Sugiyama, O. and Kaneko, S., "XPS Analysis of p-n

- Junction in p-n Joined Silicon-Germanium Semiconductor Formed by Pulse-Current Sintering,” p.234, Abstr. the 128th Meeting on Japan Inst. Metals, Tokyo (2001).
- (3) Otake, M., Isobe, K. and Sato, K., “XPS Analysis of p-n Junction in p-n Joined Silicon-Germanium Semiconductor Formed by Pulse-Current Sintering,” Abstr. the 6th Meeting on SPS Forum, Okinawa (2001).
- (4) Otake, M., Isobe, K., Sato, K., Kakuta, N., Watanabe, M., Tsuji, T. and Kaneko, S., “Power output Characteristics of Integral SiGe Thermoelectric Element,” pp.69-70, Abstr. the 18th Meeting on Ceram. Soc. Japan. Kanto Branch, Shizuoka (2002).
- (5) Otake, M., Isobe, K., Sato, K., Kakuta, N., Watanabe, M., Tsuji, T. and Kaneko, S., “Output Evaluation and Shape Optimization of Integral SiGe Thermoelectric Element,” pp.108-109, Abstr. Jpn. Symposium on Thermoelectric Conversion (TEC), Tokyo (2002).
- (6) Otake, M., Sato, K., Sugiyama, O. and Kaneko, S., “Preparation of p- and n-Type Si-Ge Powders for Thermoelectric Element by a Gas-Atomizing Method,” p.67, Abstr. the 5th International Meeting of Pacific Rim Ceramic Societies, Nagoya (2003).
- (7) Otake, M., Sato, K., Sugiyama, O. and Kaneko, S., “Pulse-Current Sintering and Thermoelectric Properties of Gas-Atomized Silicon-Germanium Powders,” p.116, Abstr. the 15th International Symposium on the Reactivity of Solids, Kyoto (2003).